MOLECULAR AND CELLULAR BIOLOGY, Nov. 2009, p. 5843–5857 Vol. 29, No. 21
0270-7306/09/$12.00 doi:10.1128/MCB.01549-08

Extracellular Signal-Regulated Kinase 1 (ERK1) and ERK2 Play Essential Roles in Osteoblast Differentiation and in Supporting Osteoclastogenesis▽†

Takehiko Matsushita,[1] Yuk Yu Chan,[1] Aya Kawanami,[1] Gener Balmes,[4] Gary E. Landreth,[2] and Shunichi Murakami[1,3]*

Department of Orthopaedics, Case Western Reserve University, 10900 Euclid Avenue, Cleveland, Ohio 44106[1]; Department of Neurosciences, Case Western Reserve University, 10900 Euclid Avenue, Cleveland, Ohio 44106[2]; Department of Genetics, Case Western Reserve University, 10900 Euclid Avenue, Cleveland, Ohio 44106[3]; and Department of Molecular Genetics, University of Texas M. D. Anderson Cancer Center, 1515 Holcombe Blvd., Houston, Texas 77030[4]

Received 3 October 2008/Returned for modification 4 January 2009/Accepted 25 August 2009

Osteoblasts and chondrocytes arise from common osteo-chondroprogenitor cells. We show here that inactivation of *ERK1* and *ERK2* in osteo-chondroprogenitor cells causes a block in osteoblast differentiation and leads to ectopic chondrogenic differentiation in the bone-forming region in the perichondrium. Furthermore, increased mitogen-activated protein kinase signaling in mesenchymal cells enhances osteoblast differentiation and inhibits chondrocyte differentiation. These observations indicate that extracellular signal-regulated kinase 1 (ERK1) and ERK2 play essential roles in the lineage specification of mesenchymal cells. The inactivation of ERK1 and ERK2 resulted in reduced beta-catenin expression, suggesting a role for canonical Wnt signaling in ERK1 and ERK2 regulation of skeletal lineage specification. Furthermore, inactivation of ERK1 and ERK2 significantly reduced *RANKL* expression, accounting for a delay in osteoclast formation. Thus, our results indicate that ERK1 and ERK2 not only play essential roles in the lineage specification of osteo-chondroprogenitor cells but also support osteoclast formation in vivo.

The extracellular signal-regulated kinase/mitogen-activated protein kinase (ERK MAPK) pathway is activated by various stimuli, including a number of growth factors and cytokines. The activation of the Raf members of MAPK kinase kinase leads to the activation of the MAPK kinase, MEK1, and MEK2. MEK1 and MEK2 then phosphorylate and activate MAPK, ERK1, and ERK2. ERK1 and ERK2 phosphorylate various cytoplasmic and nuclear target proteins, ranging from cytoplasmic adaptor proteins and transcription factors to kinases, including ribosomal S6 kinase (RSK) (4, 17, 18, 23, 36, 46). In this pathway, multiple mutations that cause syndromes with various skeletal manifestations have recently been identified. Missense-activating mutations in KRAS, BRAF, MEK1, and MEK2 have been identified in Costello, Noonan, LEOPARD, and Cardio-facio-cutaneous syndromes, while loss-of-function mutations in RSK2, a kinase downstream of ERK1 and ERK2, cause Coffin-Lowry syndrome (2, 42). These observations highlight the importance of the ERK MAPK pathway in human skeletal development.

Both chondrocytes and osteoblasts arise from common osteo-chondro progenitor cells. Bone growth is achieved through two major ossification processes, endochondral ossification and intramembranous ossification, in which chondrocytes and osteoblasts are involved (5, 13, 30, 31, 38). In normal endochondral ossification, the skeletal element is formed as a cartilaginous template that is subsequently replaced by bone. Condensed mesenchymal cells differentiate into chondrocytes. Chondrocytes first proliferate in columnar stacks to form the growth plate and then exit the cell cycle and differentiate into hypertrophic chondrocytes. Hypertrophic chondrocytes are removed by apoptotic cell death, and the cartilaginous matrix is resorbed by chondroclasts/osteoclasts and replaced by trabecular bone. Chondroclast/osteoclast formation is supported by receptor activator of nuclear factor-kappa B ligand (RANKL) secreted from osteoblasts and bone marrow stromal cells (16, 45). In intramembranous ossification, mesenchymal cells directly differentiate into bone-forming osteoblasts; cortical bone is formed by osteoblasts that arise from the osteo-chondroprogenitor cells in the perichondrium. Previous studies with mice have indicated that the ERK MAPK signaling cascade participates in chondrocyte and osteoblast differentiation. Expression of a constitutively active mutant of MEK1 in chondrocytes caused a dwarf phenotype and inhibited hypertrophic chondrocyte differentiation (28). In addition, expression of a constitutively active mutant of MEK1 in mature osteoblasts accelerated bone development, whereas dominant-negative MEK1 was inhibitory at the embryonic stage (11). The roles of ERK/MAPK signaling in mesenchymal cell differentiation require further investigation. In the current study, using the Cre-*loxP* system, we examined the roles of ERK1 and ERK2 in early steps of chondrocyte and osteoblast differentiation and two major ossification processes, endochondral ossification and intramembranous ossification, by generating loss-of-function models. In addition to the loss-of-function models, we also generated a gain-of-function model (mice that overexpress a constitutively active mutant of MEK1 in undifferentiated mes-

* Corresponding author. Mailing address: Dept. of Orthopaedics, Case Western Reserve University, 2109 Adelbert Road, BRB 329, Cleveland, OH 44106. Phone: (216) 368-1371. Fax: (216) 368-1332. E-mail: shun@case.edu.

† Supplemental material for this article may be found at http://mcb.asm.org/.

▽ Published ahead of print on 8 September 2009.

enchymal cells) and examined the roles of ERK/MAPK signaling in osteo-chondro progenitor cells.

We show here that ERK1 and ERK2 are essential for osteoblast differentiation and that ERK1 and ERK2 inhibit ectopic cartilage formation in the perichondrium. We also show that increased MAPK signaling in osteo-chondroprogenitor cells inhibits cartilage formation and that increased MAPK signaling in the perichondrium stimulates bone formation. Furthermore, inactivation of ERK1 and ERK2 significantly reduced *RANKL* expression, accounting for a delay in osteoclast formation. Thus, our results indicate that ERK1 and ERK2 not only play essential roles in the lineage specification of osteo-chondroprogenitor cells but also support osteoclast formation in vivo.

MATERIALS AND METHODS

Mutant animals. The institutional animal care and use committee of Case Western Reserve University approved all animal procedures. All animal care and use were performed in accordance with the institutional animal use methods and policies. *ERK1*-deficient mice and *Prx1-Cre* and *Col2a1-Cre* transgenic mice were described previously (21, 32, 37). The floxed *ERK2* allele was created by inserting *loxP* sites flanking exon2 (35). To generate *Prx1-MEK1* transgenic mice, the cDNA for FLAG-tagged MEK1(S218/222E, Δ32-51) and an *IRES-LacZ* cassette were cloned downstream of a 2.4-kb *Prx1* promoter (24, 28). The construct was microinjected into the pronuclei of fertilized C57BL/6-DBA/2 hybrid eggs. *ROSA-LacZ* reporter mice were purchased from Jackson Laboratories (41).

In situ hybridization, immunohistochemistry, TRAP staining, and BrdU incorporation assay. In situ hybridization was performed using ^{35}S-labeled riboprobes. Nuclei were visualized with Hoechst 33258. Immunohistochemical staining was performed using a PicTure kit (Invitrogen) or MM biotinylation kit (Biocare). The following antibodies were used: ERK1/2 (Santa Cruz), type X collagen (Quartett), FLAG M5 (Sigma), and β-catenin (BD) antibodies. For immunofluorescent detection of ERK1/2, Alexa Fluor 594-conjugated secondary antibody (Invitrogen) was used. Fluorescence-based tartrate-resistant acid phosphatase (TRAP) staining and alkaline phosphatase staining were performed using ELF97 (Invitrogen) as a phosphatase substrate (6, 10). To reduce background, TRAP staining using ELF97 was performed in the presence of 50 mM tartrate. Naphthol AS-BI phosphoric acid-based TRAP staining was performed using an acid phosphatase leukocyte kit (Sigma). For examining cell proliferation, mice were injected intraperitoneally with BrdU. Embryos were harvested 4 h after injection. BrdU incorporation was detected using a BrdU staining kit (Zymed). All images were acquired with Leica DM 6000B and DM IRB microscopes. Photographs were taken with a digital camera (DC500; Leica) using Leica Application Suite 1.3 software. The signal of in situ hybridization in dark-field images was colored using Photoshop software (Adobe), and brightness and contrast were adjusted by applying brightness/contrast adjustments to the whole image, with the strict intent of not obscuring, eliminating, or misrepresenting any information present in the original, including background. For in situ hybridization, the signal images were overlaid on images of Hoechst 33258.

RNA analysis and semiquantitative and real time PCR. Total RNA was isolated using an RNeasy kit (Qiagen). RNA was reverse transcribed to cDNA with a high-capacity cDNA archive kit (Applied Biosystems). Real-time PCR was performed with the Applied Biosystems 7500 real-time PCR detection system. TaqMan probe sets were designed and synthesized by Applied Biosystems (*Erk2*, Mm00442479_m1; *Rankl*, Mm00441908_m1; *Opg*, Mm00435452_m1; *Dkk1*, Mm00438422_m1; *Tcf1*, Mm03053891_s1; *Cbfb*, Mm00491551_m1; c-*Fos*, Mm00487425_m1; *Fra1*, Mm00487429_m1; *Fra2*, Mm00484442_m1; *JunB*, Mm00492781_s1; *Krox20*, Mm00456650_m1; *Col2a1*, Mm01309562_g1; *Col10a1*, Mm00487041_m1; *Gapdh*, 4352932E). To compare gene expression levels, the comparative cycle threshold method was used. *Gapdh* was used as an endogenous control to correct for potential variation in RNA loading or in efficiency of amplification. Semiquantitative PCR was performed with the Applied Biosystems 9700 GeneAmp PCR system, using the following primer sets: for *Runx2*, 5′-GAACCAAGAAGGCA CAGACA-3′ (forward) and 5′-AACTGCCTGGGGTCTGAAAA-3′ (reverse) (PCR product, 452 bp); for *Osteocalcin*, 5′-CTCTGTCTCTCTGACC TCACAG-3′ (forward) and 5′-CAGGTCCTAAATAGTGATACCG-3′ (reverse) (PCR product, 252 bp); for *BSP*, 5′-GAAACGGTTTCCAGTCCA G-3′ (forward) and 5′-CTGAAACCCGTTCAGAAGG-3′ (reverse) (PCR product, 568 bp); for *Col1a2*, 5′-TGAAGTGGGTCTTCCAGGTC-3′ (forward) and 5′-GACCAGGCTCACCAACAAGT-3′ (reverse) (PCR product, 200 bp); for *Alkaline phosphatase*, 5′-AATGCCCTGAAACTCCAAAAGC-3′ (forward) and 5′-CCTCTGGTGGCATCTCGTTATC-3′ (reverse) (PCR product, 472 bp); and for *Gapdh*, 5′-ACCACAGTCCATGCCATCAC-3′ (forward) and 5′-TCCACCACCCTGTTGCTGTA-3′ (reverse) (PCR product, 452 bp). The band intensities were compared, while the band intensity and cycle numbers are linear.

Cell culture. Primary rib chondrocytes and calvarium osteoblasts were isolated as described previously (12, 28). Cells were infected with adenovirus (Ad) expressing Cre, green fluorescent protein (GFP) (Gene Transfer Vector Core, University of Iowa), or constitutively active MEK1 (Vector Biolabs) at a multiplicity of infection of 150 to 200. Osteoblasts were grown in differentiation medium (alpha minimum essential medium, 10% fetal calf serum, 5 mM β-glycerophosphate, 100 μg/ml ascorbic acid). Alizarin red and von Kossa staining were done by following standard protocols. For in vitro osteoclast differentiation, spleen cells were isolated and cultured in alpha minimal essential medium supplemented with 10% fetal calf serum, 10 ng/ml RANKL (R&D), and L929 cell-conditioned medium containing macrophage colony-stimulating factor (M-CSF).

Western blot analysis. Total cellular protein was prepared by lysing cells in 62.5 mM Tris-HCl (pH 6.8), 2% sodium dodecyl sulfate, 10% glycerol, 1 mM sodium orthovanadate, 1 mM sodium fluoride, 1 mM β-glycerophosphate, supplemented with proteinase inhibitor cocktail Complete Mini (Roche). Protein concentrations were determined by a bicinchoninic acid protein assay kit (Pierce). Twenty to thirty micrograms of protein was separated by 10% sodium dodecyl sulfate-polyacrylamide gel electrophoresis and electrophoretically transferred to polyvinylidene difluoride filters (Millipore). The filters were blocked in 5% nonfat dry milk in Tris-buffered saline (pH 7.5) containing 0.1% Tween 20 and then incubated with the following antibodies: ERK1 and ERK2 (Santa Cruz), Osterix (Santa Cruz), ATF4 (Santa Cruz), RSK2 (Cell Signaling Technology), and β-actin (Cell Signaling Technology) antibodies. Filters were then incubated with the second antibody (horseradish peroxidase-conjugated anti-rabbit or anti-goat immunoglobulin G), and the signal was detected by enhanced chemiluminescence (Pierce). Images were captured using a KODAK Image Station 4000MM device.

RESULTS

Inactivation of *ERK2* in mesenchymal cells of *ERK1*-null mice causes severe limb deformity and bone defects. We first analyzed *ERK1*-null mice and *ERK2*$^{flox/flox}$; *Prx1-Cre* mice, in which *ERK2* was inactivated in the limb and head mesenchyme by using the *Prx1-Cre* transgene. These mice did not show obvious skeletal abnormalities (data not shown). To totally inactivate *ERK1* and *ERK2*, we further inactivated *ERK2* in the *ERK1*-null background. *ERK1*$^{-/-}$; *ERK2*$^{flox/flox}$; *Prx1-Cre* mice were born at the expected Mendelian ratio. Skeletal preparation of *ERK1*$^{-/-}$; *ERK2*$^{flox/flox}$; *Prx1-Cre* mice by use of alcian blue and alizarin red staining showed severe limb deformity at postnatal day 0 (P0) (Fig. 1A; see also Fig. S1 in the supplemental material). In addition, *ERK1*$^{-/-}$; *ERK2*$^{flox/flox}$; *Prx1-Cre* mice showed bone defects in the calvaria. The lambdoid suture did not close at least up to P12 (Fig. 1B). Histological examination showed no distinct cortical bone formation in the humeri of *ERK1*$^{-/-}$; *ERK2*$^{flox/flox}$; *Prx1-Cre* mice at P5 (Fig. 1C). *ERK2* inactivation was confirmed to occur in the tibiae, femurora, and humeri of *ERK1*$^{-/-}$; *ERK2*$^{flox/flox}$; *Prx1-Cre* embryos at embryonic day 16.5 (E16.5) by real-time PCR (Fig. 1D and data not shown). *ERK2* mRNA was decreased about 90% compared with the level in littermate *ERK1*$^{-/-}$; *ERK2*$^{flox/flox}$ embryos. The inactivation of ERK1 and ERK2 was also confirmed by immunohistochemistry using an antibody that recognizes both ERK1 and ERK2 (Fig. 1E). Immunoreactivity of chondrocytes and cells in the bone-forming area was significantly reduced in *ERK1*$^{-/-}$; *ERK2*$^{flox/flox}$; *Prx1-Cre* mice. These

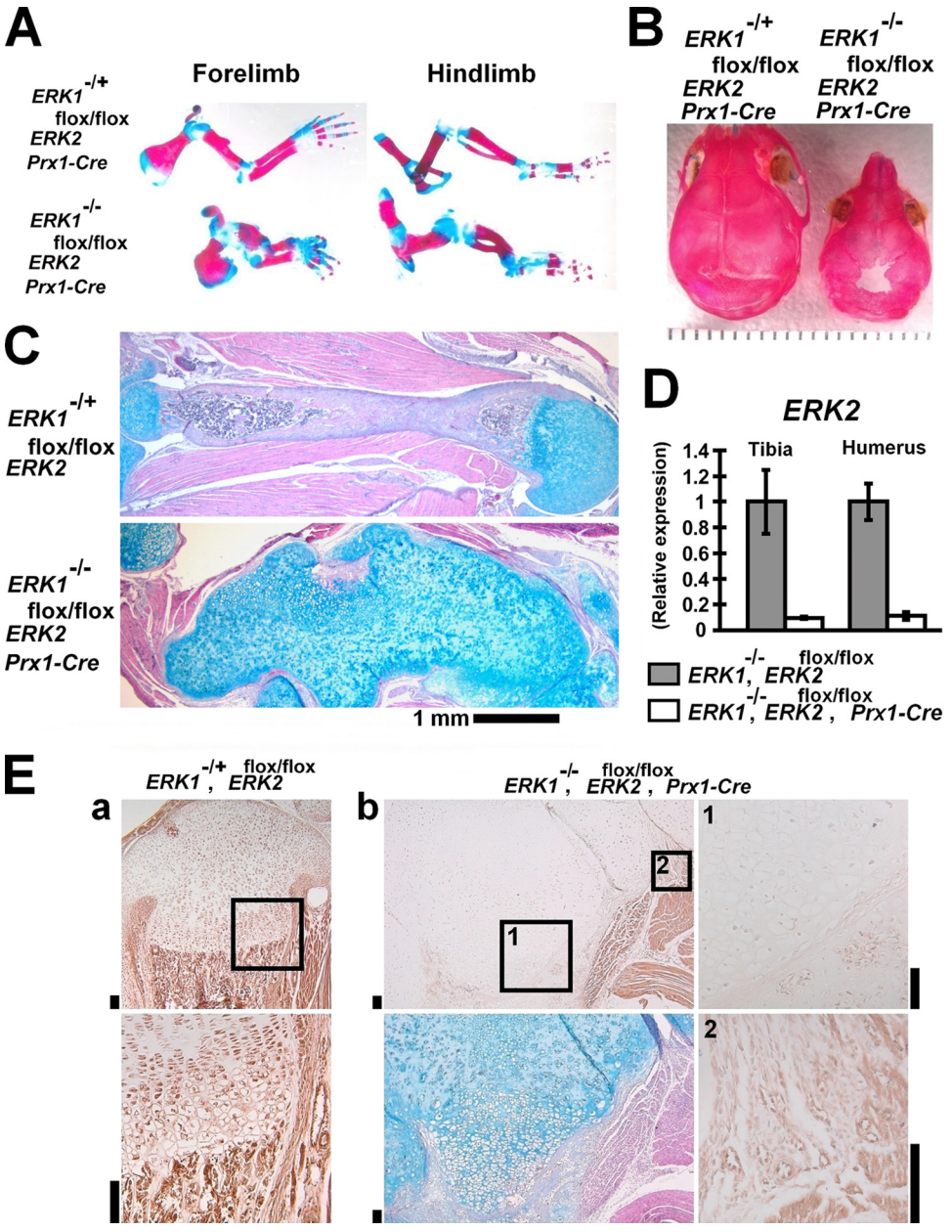

FIG. 1. *ERK1*$^{-/-}$; *ERK2*$^{flox/flox}$; *Prx1-Cre* embryos and mice. (A) Skeletal preparation after alizarin red and alcian blue staining at P1. Limbs were severely deformed in *ERK1*$^{-/-}$; *ERK2*$^{flox/flox}$; *Prx1-Cre* mice. (B) Skeletal preparation of the cranium after alizarin red staining. *ERK1*$^{-/-}$; *ERK2*$^{flox/flox}$; *Prx1-Cre* mice showed bone defects in the calvaria at P12. (C) Hematoxylin, eosin, and alcian blue staining of the humerus showing an absence of the primary ossification center and cortical bone formation in *ERK1*$^{-/-}$; *ERK2*$^{flox/flox}$; *Prx1-Cre* mice at P5. (D) Real-time PCR showed *ERK2* inactivation in the tibiae and humeri of *ERK1*$^{-/-}$; *ERK2*$^{flox/flox}$; *Prx1-Cre* embryos at E16.5. (E) Immunohistochemistry using anti-ERK1 and ERK2 antibody showed reduced immunoreactivity in chondrocytes and cells in the bone-forming region of tibiae of *ERK1*$^{-/-}$; *ERK2*$^{flox/flox}$; *Prx1-Cre* mice at P5. (a) *ERK1*$^{-/+}$; *ERK2*$^{flox/flox}$ mice. The boxed area in the upper panel is magnified in the lower panel. (b) *ERK1*$^{-/-}$; *ERK2*$^{flox/flox}$; *Prx1-Cre* mice. The upper left panel shows immunostaining for ERK1 and ERK2. Boxed areas 1 and 2 are magnified in the corresponding right panels. While chondrocytes showed reduced immunoreactivity (boxed area 1), endothelial cells show positive staining (boxed area 2). The lower left panel shows alcian blue, hematoxylin, and eosin staining of a neighboring section. Bars indicate 100 μm.

observations indicate that ERK1 and ERK2 are essential for bone formation.

ERK1 and ERK2 are essential for osteoblast differentiation. To examine osteoblast differentiation, we performed in situ hybridization analyses. Early osteoblast marker *Col1a1* and master transcription factors for osteoblast differentiation *Runx2*, *Osterix*, and *Atf4* were normally expressed in the long bones and calvaria of *ERK1*$^{-/-}$; *ERK2*$^{flox/flox}$; *Prx1-Cre* mice, indicating that ERK1 and ERK2 are not required for their expression (Fig. 2A and C and data not shown). However, the expression of *Osteocalcin*, a marker of mature osteoblasts, was undetectable in the long bones and calvaria of *ERK1*$^{-/-}$;

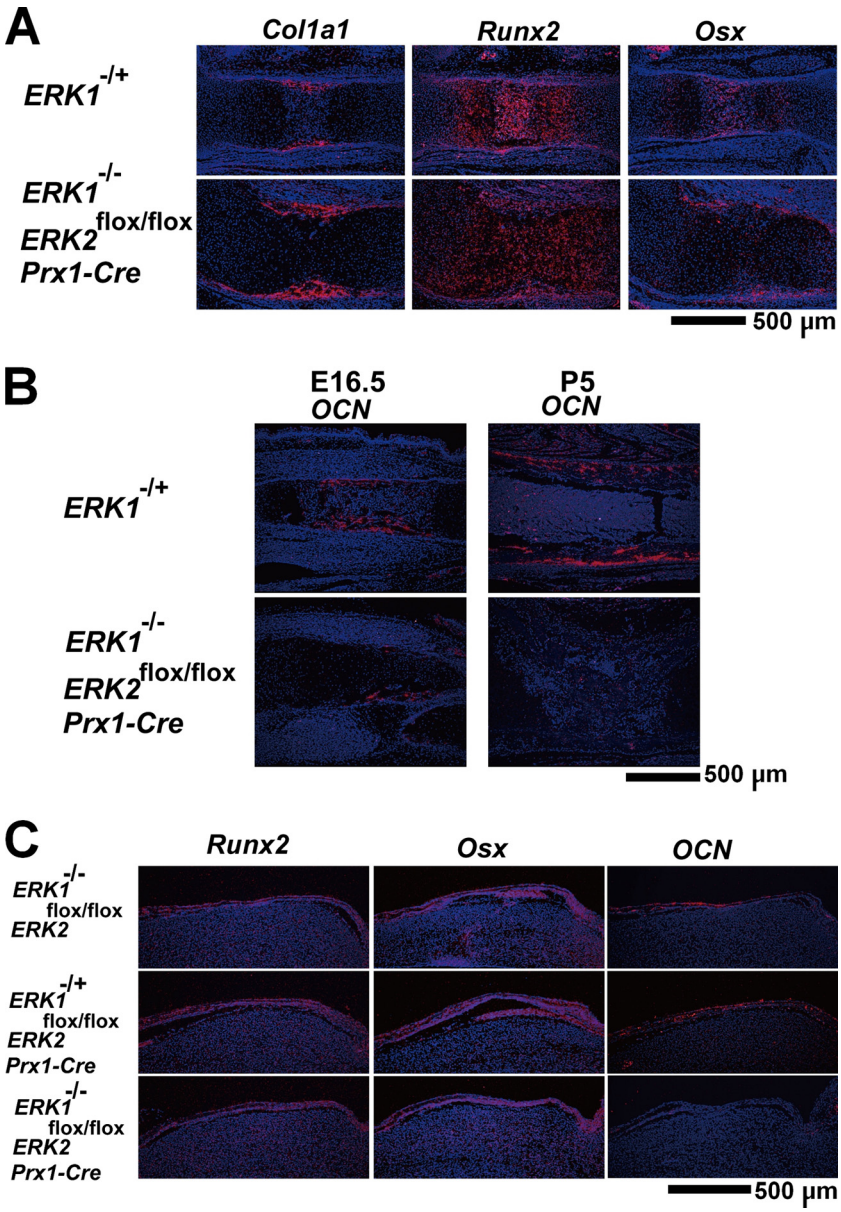

FIG. 2. In situ hybridization analyses of the femur (A, B) and calvaria (C), showing normal levels of *Col1a1*, *Runx2*, and *Osterix* (*Osx*) expression and markedly decreased *Osteocalcin* (*OCN*) expression in *ERK1*$^{-/-}$; *ERK2*$^{flox/flox}$; *Prx1-Cre* embryos and mice. (A) E15.5; (B) E16.5 and P5; (C) P1.

ERK2$^{flox/flox}$; *Prx1-Cre* mice (Fig. 2B and C). Because *Osterix* regulates *Osteocalcin* expression downstream of *Runx2*, these observations indicate that osteoblast differentiation was arrested after *Osterix* expression and before differentiation into fully mature osteoblasts.

To examine whether the block in osteoblast differentiation is due to the cell autonomous effects of *ERK1* and *ERK2* inactivation, we isolated calvarium osteoblasts from *ERK1*$^{-/-}$; *ERK2*$^{flox/flox}$ embryos. The cells were infected with Ad expressing Cre recombinase (Ad-Cre) or a control virus expressing GFP (Ad-GFP). Reverse transcription-PCR showed marked reduction of *Osteocalcin* and *Bsp* expression in cells infected with Ad-Cre, while *Alkaline phosphatase* expression was slightly reduced and *Col1a2* expression remained unaltered (Fig. 3A). These observations indicate that the block in osteoblast differentiation is cell autonomous, and ERK1 and ERK2 are required for osteoblast differentiation into mature osteoblasts. Consistent with in vivo observations, the inactivation of *ERK1* and *ERK2* did not abolish *Runx2* mRNA. In addition, *ERK1* and *ERK2* inactivation did not affect Osterix, ATF4, and RSK2 protein expression (Fig. 3B). The block in osteoblast differentiation was also confirmed by von Kossa staining (Fig. 3C).

We also isolated the tibiae, femurora, and humeri of E16.5 embryos and examined expression of transcription factors implicated in osteoblast differentiation by real-time PCR. We found that a number of transcription factors were downregulated in the skeletal elements of *ERK1*$^{-/-}$; *ERK2*$^{flox/flox}$; *Prx1-*

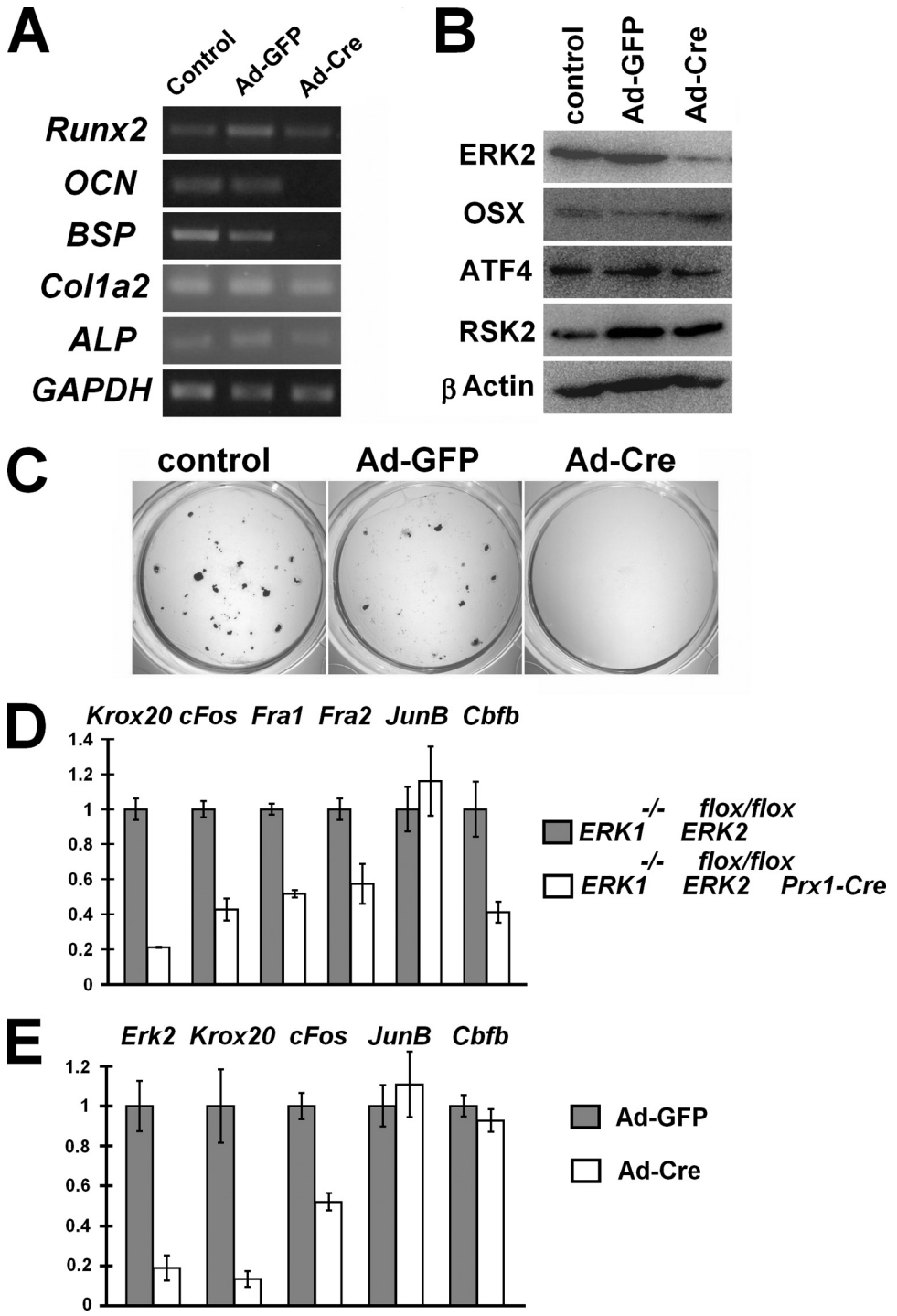

FIG. 3. (A) Semiquantitative reverse transcription-PCR showing reduced *Osteocalcin* (*OCN*) and *Bone sialoprotein* (*BSP*) expression in primary *ERK1*$^{-/-}$; *ERK2*$^{flox/flox}$ calvarium mesenchymal cells that were infected with Ad expressing Cre recombinase (Ad-Cre). Primary calvarium mesenchymal cells were isolated from E15.5 *ERK1*$^{-/-}$; *ERK2*$^{flox/flox}$ embryos and infected with Ad-Cre or Ad expressing GFP (Ad-GFP). RNA was extracted 20 days after infection. (B) Western blot analysis showing Osterix (OSX), ATF4, and RSK2 expression in primary *ERK1*$^{-/-}$; *ERK2*$^{flox/flox}$ calvarium cells that were infected with Ad-Cre or Ad-GFP. ERK2 expression was inhibited 80% by Ad-Cre infection, while Osterix, ATF4, and RSK2 expression remained largely unaffected. Total cell lysates were prepared 10 days after infection. (C) von Kossa staining of *ERK1*$^{-/-}$; *ERK2*$^{flox/flox}$ calvarium cell cultures 20 days after infection with Ad-Cre or Ad-GFP. Ad-Cre infection inhibited mineralization. (D) Real-time PCR analysis showed reduced *Krox20*, c-*Fos*, *Fra1*, *Fra2*, and *Cbfb* expression in the humeri of *ERK1*$^{-/-}$; *ERK2*$^{flox/flox}$; *Prx1-Cre* embryos at E16.5, while *JunB* was not affected. Real-time PCR analysis of the tibia and femur showed similar results. (E) Real time PCR analysis showed reduced *Erk2*, *Krox20*, and c-*Fos* expression in *ERK1*$^{-/-}$; *ERK2*$^{flox/flox}$ calvarium cells infected with Ad-Cre. *ERK1*$^{-/-}$; *ERK2*$^{flox/flox}$ calvarium cells were infected with Ad-Cre or Ad-GFP, and RNA was extracted 9 days after infection.

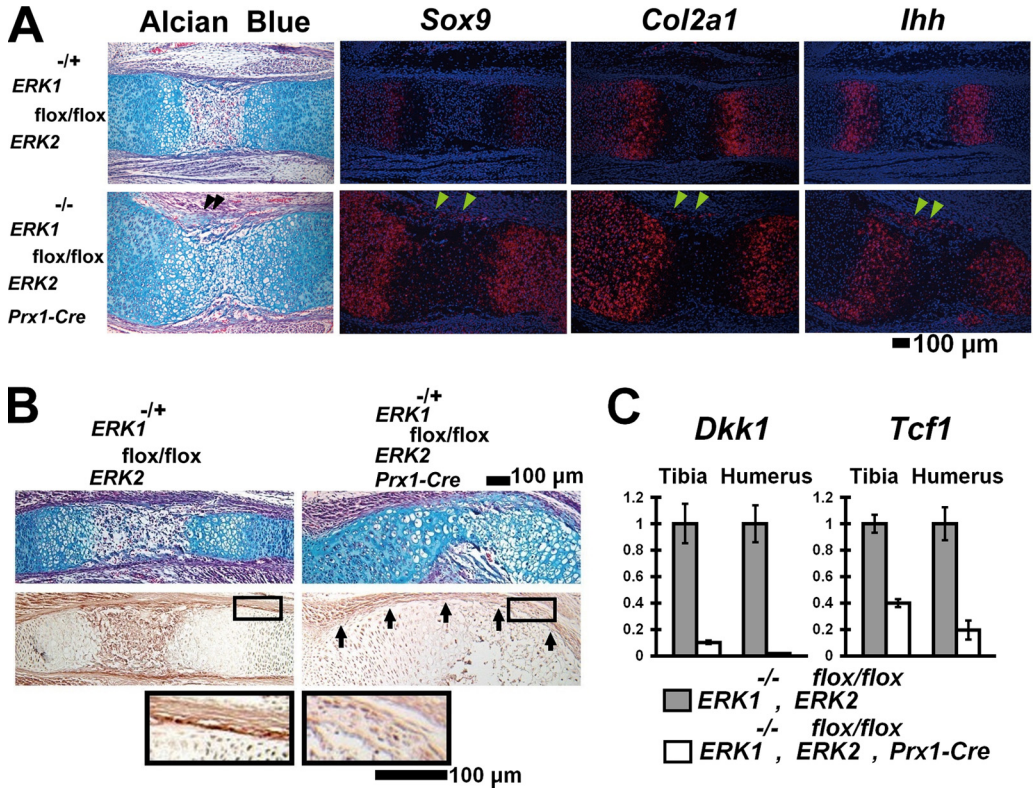

FIG. 4. Ectopic cartilage formation in the perichondria of *ERK1*$^{-/-}$; *ERK2*$^{flox/flox}$; *Prx1-Cre* embryos. (A) Alcian blue staining and in situ hybridization of the femur at E15.5. The ectopic cartilage (arrowheads) in the perichondrium expresses *Sox9*, *Col2a1*, and *Indian hedgehog* (*Ihh*). (B) Alcian blue staining (top panel) and immunohistochemical staining of the radius for β-catenin (middle panel). *ERK1*$^{-/-}$; *ERK2*$^{flox/flox}$; *Prx1-Cre* embryos showed reduced β-catenin protein levels in the perichondrium at E16.5 (arrows). The boxed area is magnified in the bottom panel. (C) *Tcf1* and *Dkk1* expression quantitated by real-time PCR. *ERK1*$^{-/-}$; *ERK2*$^{flox/flox}$; *Prx1-Cre* embryos showed reduced *Tcf1* and *Dkk1* expression in the tibia and humerus at E16.5.

Cre embryos. *Krox20* was strongly inhibited in bones lacking ERK1 and ERK2 (Fig. 3D). In addition, AP-1 family members *Fra1*, *Fra2*, and c-*Fos* were all downregulated in bones lacking ERK1 and ERK2. In contrast, *JunB* expression remained unchanged, indicating that the downregulation of *Krox20*, *Fra1*, *Fra2*, and c-*Fos* is not a consequence of general suppression of transcription. Furthermore, *Cbfb*, which encodes a coregulator of runt domain transcriptional factors, was also downregulated in bones lacking ERK1 and ERK2 (27, 47). Therefore, the severe bone phenotype of *ERK1*$^{-/-}$; *ERK2*$^{flox/flox}$; *Prx1-Cre* mice likely involves multiple regulatory factors of osteoblast differentiation. Consistent with these observations, at least *Krox20* and c-*Fos* were strongly inhibited in calvarium cells infected with Ad-Cre (Fig. 3E).

Inactivation of ERK1 and ERK2 in mesenchymal cells causes ectopic cartilage formation in the perichondrium. Interestingly, we observed ectopic cartilage formation in the perichondria of *ERK1*$^{-/-}$; *ERK2*$^{flox/flox}$; *Prx1-Cre* mice (Fig. 4A). The ectopic cartilage formation was observed as early as E13.5 in the mutant humerus (see Fig. S2B in the supplemental material). Cells in the ectopic cartilage expressed a master transcription factor for chondrocyte differentiation, *Sox9*, and a cartilage-specific marker, *Col2a1*, indicating chondrogenic differentiation. These observations suggest that osteo-chondroprogenitor cells in the perichondrium were blocked in their differentiation into osteoblasts and instead differentiated into chondrocytes. Interestingly, the cells in the ectopic cartilage also expressed markers for prehypertrophic chondrocytes (*Indian hedgehog* [*Ihh*] and *Parathyroid hormone/Parathyroid hormone-related peptide receptor*) as well as markers for hypertrophic chondrocytes (*Col10a1* and *Mmp13*) (Fig. 4A and data not shown; see also Fig. S2G and H in the supplemental material). It is possible that chondrocytes in the ectopic cartilage accelerated differentiation into hypertrophic chondrocytes in the absence of ERK1 and ERK2.

Since the inactivation of β-catenin in mesenchymal cells causes similar ectopic cartilage formation in the perichondrium (7, 12, 34), we examined β-catenin expression by immunohistochemistry. Strong β-catenin expression was observed in the bone-forming region of the periostea and perichondria of control embryos at E15.5 (Fig. 4B). In contrast, β-catenin staining was decreased in the periostea and perichondria of *ERK1*$^{-/-}$; *ERK2*$^{flox/flox}$; *Prx1-Cre* embryos. We further examined *Tcf1* and *Dkk1* expression by real-time PCR, because both *Tcf1* and *Dkk1* expression depends on intact β-catenin signaling (12, 34). We observed strong inhibition of *Tcf1* and *Dkk1* expression, supporting the notion that β-catenin signaling is reduced in the skeletal elements (Fig. 4C).

Ectopic chondrocyte differentiation in the perichondrium in association with a block in osteoblast differentiation has been

also reported to occur in *Osterix*-null mice and in mice in which Ihh signaling is disrupted (22, 29). *Osterix*, *Ihh*, and its downstream target *Patched* were normally expressed in the skeletal elements of *ERK1*$^{-/-}$; *ERK2*$^{flox/flox}$; *Prx1-Cre* embryos (Fig. 2A and 4A; see also Fig. S2G in the supplemental material). In addition, coexpression of a constitutively active mutant of MEK1 did not affect the transcriptional activity of Osterix in transient-transfection experiments in vitro (data not shown). These observations suggest that *Osterix* and *Ihh* signaling are not affected by MAPK signaling.

Inactivation of ERK1 and ERK2 caused an expansion of terminally differentiated chondrocytes in the growth plates and decreased osteoclasts. The inactivation of ERK1 and ERK2 resulted in a remarkable widening of the zone of hypertrophic chondrocytes in the growth plate (Fig. 5A). Some of the epiphyseal chondrocytes closer to the articular surface stained positive for type X collagen, suggesting accelerated hypertrophy. This notion is further supported by an increase in *Col10a1* expression in *ERK1*$^{-/-}$; *ERK2*$^{flox/flox}$ primary chondrocytes that were infected with Ad-Cre (see Fig. 7C). In addition, in situ hybridization indicated that the widening of the zone of hypertrophic chondrocytes is associated with a remarkable expansion of terminally differentiated hypertrophic chondrocytes (Fig. 5B). Although the matrix showed intense staining with anti-type X collagen antibody, these cells expressed *Col10a1* at a reduced level and instead expressed markers for terminally differentiated hypertrophic chondrocytes (*Vegf*, *Mmp13*, and *Osteopontin*). These observations suggest that the expansion of the hypertrophic zone is caused by impaired removal of terminally differentiated hypertrophic chondrocytes. Terminal deoxynucleotidyltransferase-mediated dUTP-biotin nick end labeling staining did not show significant difference between control and mutant mice, suggesting that chondrocyte apoptosis is not affected (data not shown).

Inactivation of ERK1 and ERK2 caused decreases in osteoclast formation and RANKL expression. We also examined osteoclasts by TRAP staining. TRAP-positive cells were decreased in the long bones of *ERK1*$^{-/-}$; *ERK2*$^{flox/flox}$; *Prx1-Cre* embryos at E16.5 (Fig. 5C), suggesting that the decreased osteoclasts account at least in part for the delayed cartilage removal in *ERK1*$^{-/-}$; *ERK2*$^{flox/flox}$; *Prx1-Cre* embryos. Consistent with the reduced number of osteoclasts, immunohistochemistry for MMP9 showed reduced staining in *ERK1*$^{-/-}$; *ERK2*$^{flox/flox}$; *Prx1-Cre* embryos (see Fig. S3A in the supplemental material).

Since osteoclastogenesis is regulated by RANKL and osteoprotegerin (OPG) produced by mesenchymal cells, we examined *RANKL* and *OPG* expression in the long bones of *ERK1*$^{-/-}$; *ERK2*$^{flox/flox}$; *Prx1-Cre* embryos. *RANKL* expression was strongly inhibited in the long bones of *ERK1*$^{-/-}$; *ERK2*$^{flox/flox}$; *Prx1-Cre* embryos, while *OPG* expression remained unaltered (Fig. 5D and data not shown). Because the *Prx1-Cre* transgene inactivates *ERK2* both in chondrocytes and in osteoblasts, we examined *RANKL* and *OPG* regulation in each cell lineage in vitro. We harvested calvarial osteoblasts and rib chondrocytes from *ERK1*$^{-/-}$; *ERK2*$^{flox/flox}$ mice and inactivated *ERK2* by infecting Ad expressing Cre recombinase. In both cell types, *ERK2* inactivation strongly inhibited *RANKL* expression, while *OPG* expression was not affected (Fig. 5E and F). Consistent with these observations, treatment with MEK inhibitor U0126 strongly inhibited *RANKL* expression in both cell types (see Fig. S3B and C in the supplemental material). These observations indicate that *RANKL* expression depends on MAPK signaling both in the osteoblast and in the chondrocyte lineages.

Since reduced osteoclastogenesis could be due to unspecific deletion of *ERK1* and *ERK2* in the osteoclast lineage, we examined ERK expression in osteoclasts of *ERK1*$^{-/-}$; *ERK2*$^{flox/flox}$; *Prx1-Cre* mice by double staining for TRAP activity and ERK protein. Fluorescence-based TRAP staining using ELF97 showed green fluorescence in osteoclasts of *ERK1*$^{-/-}$; *ERK2*$^{flox/flox}$; *Prx1-Cre* mice at P0 (Fig. 5G). The staining intensity for ERK is similar to that of osteoclasts of littermate *ERK1*$^{-/-}$; *ERK2*$^{flox/flox}$ mice (data not shown). To check the activity of the *Prx1-Cre* transgene in the monocyte/macrophage lineage, we further isolated spleen cells from *ROSA-LacZ* reporter mice harboring the *Prx1-Cre* transgene and control *ROSA-LacZ* reporter mice without the *Prx1-Cre* transgene. These cells were induced to differentiate into osteoclast-like cells in the presence of M-CSF and RANKL. X-Gal (5-bromo-4-chloro-3-indolyl-β-D-galactopyranoside) staining followed by TRAP staining showed no X-Gal staining in TRAP-positive osteoclast-like cells, indicating that the *Prx1-Cre* transgene is not active during in vitro osteoclast differentiation (Fig. 5H).

To further exclude the possibility that the reduced osteoclast formation in *ERK1*$^{-/-}$; *ERK2*$^{flox/flox}$; *Prx1-Cre* mice is due to defects in osteoclast precursor cells, we isolated spleen cells from *ERK1*$^{-/-}$; *ERK2*$^{flox/flox}$; *Prx1-Cre* and littermate *ERK1*$^{-/-}$; *ERK2*$^{flox/flox}$ mice at P0. Spleen cells from *ERK1*$^{-/-}$; *ERK2*$^{flox/flox}$; *Prx1-Cre* mice formed osteoclast-like multinucleated giant cells in the presence of M-CSF and RANKL, similar to *ERK1*$^{-/-}$; *ERK2*$^{flox/flox}$ cells (Fig. 5I and data not shown). These giant cells displayed TRAP activity and expressed ERK, similar to *ERK1*$^{-/-}$; *ERK2*$^{flox/flox}$ cells. These observations further support the notion that reduced osteoclastogenesis in *ERK1*$^{-/-}$; *ERK2*$^{flox/flox}$; *Prx1-Cre* embryos is due to reduced support from mesenchymal cells.

ERK1 and ERK2 inactivation in chondrocytes causes severe chondrodysplasia. To further examine the roles of ERK1 and ERK2 in differentiated chondrocytes, we inactivated *ERK2* in chondrocytes of *ERK1*-null mice by using the *Col2a1-Cre* transgene. *ERK1*$^{-/-}$; *ERK2*$^{flox/flox}$; *Col2a1-Cre* mice died immediately after birth, presumably due to respiratory insufficiency caused by the defective rib cage. We obtained *ERK1*$^{-/-}$; *ERK2*$^{flox/flox}$; *Col2a1-Cre* mice at a Mendelian ratio at E18.5. The inactivation of ERK1 and ERK2 in chondrocytes was confirmed by immunofluorescence using the antibody that recognizes both ERK1 and ERK2 (Fig. 6A). We further confirmed ERK expression in osteoblasts and osteoclasts of *ERK1*$^{-/-}$; *ERK2*$^{flox/flox}$; *Col2a1-Cre* embryos by performing ELF97-based fluorescent alkaline phosphatase staining and TRAP staining along with immunofluorescence for ERK (Fig. 6B and C). The fluorescent signal for ERK was indistinguishable from that of control *ERK1*$^{-/-}$; *ERK2*$^{flox/flox}$ embryos (data not shown). Consistent with the normal expression of ERK in osteoblasts, calvarium osteoblasts isolated from *ERK1*$^{-/-}$; *ERK2*$^{flox/flox}$; *Col2a1-Cre* embryos showed mineralization, similar to *ERK1*$^{+/-}$; *ERK2*$^{flox/flox}$ cells, in vitro (see Fig. S4 in the supplemental material).

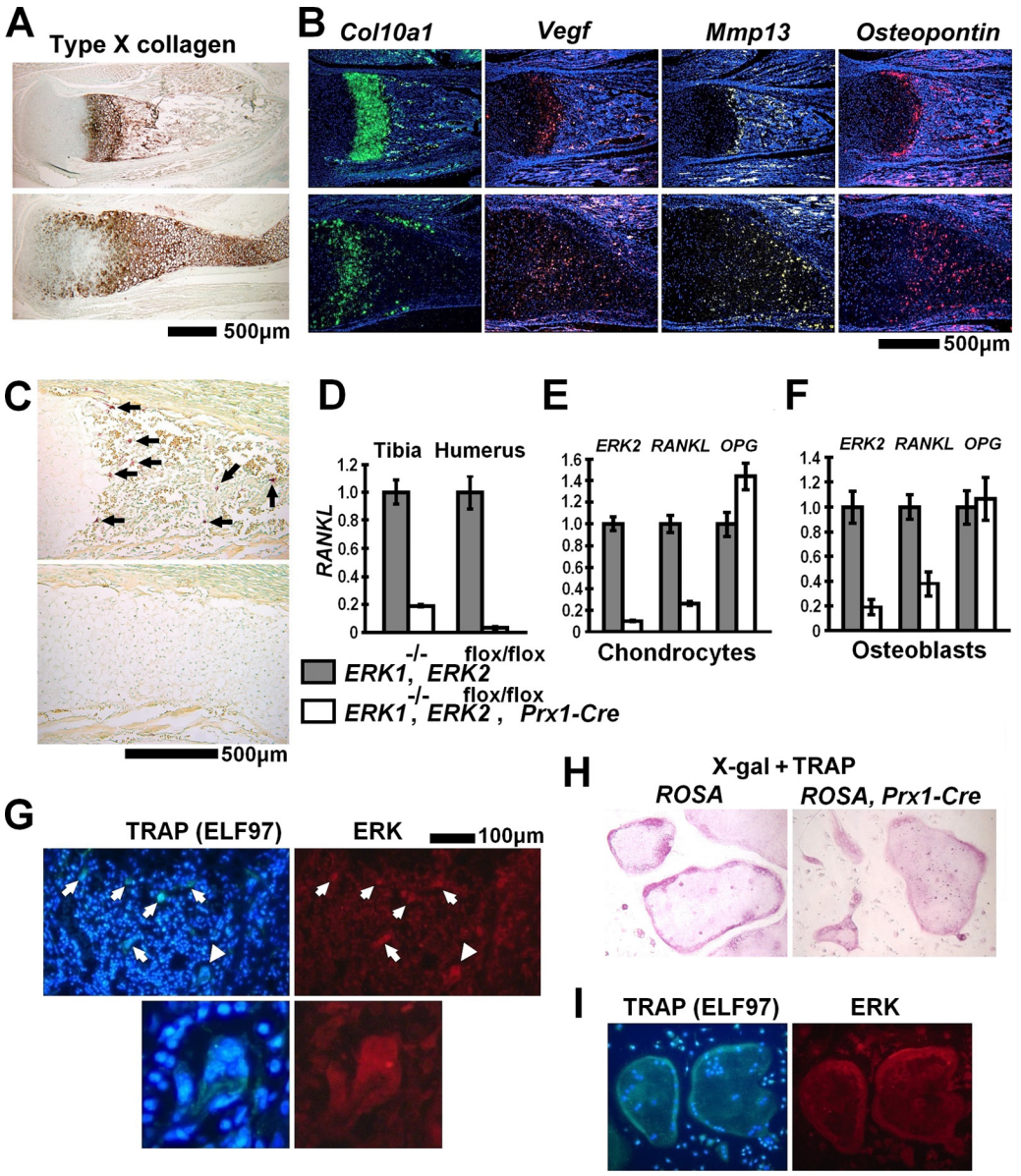

FIG. 5. Delayed formation of primary ossification centers in *ERK1*$^{-/-}$; *ERK2*$^{flox/flox}$; *Prx1-Cre* mice. (A) Immunohistochemistry for type X collagen showed a widening of the zone of hypertrophic chondrocytes in the tibiae of *ERK1*$^{-/-}$; *ERK2*$^{flox/flox}$; *Prx1-Cre* mice at P0. (B) In situ hybridization for *Col10a1*, *Vegf*, *Mmp-13*, and *Osteopontin* showed an expansion of terminally differentiated chondrocytes in the hypertrophic zone of the tibia at P0. (C) TRAP staining showed an absence of TRAP-positive cells in the tibiae of *ERK1*$^{-/-}$; *ERK2*$^{flox/flox}$; *Prx1-Cre* embryos at E16.5. Arrows indicate TRAP-positive cells. The upper images in panels A, B, and C show *ERK1*$^{-/-}$, and the lower images show *ERK1*$^{-/-}$; *ERK2*$^{flox/flox}$; *Prx1-Cre* mice. (D) Real-time PCR showed reduced *RANKL* expression in the tibiae and humeri of *ERK1*$^{-/-}$; *ERK2*$^{flox/flox}$; *Prx1-Cre* embryos at E16.5. (E, F) *ERK2*, *RANKL*, and *Osteoprotegerin* (*OPG*) expression examined by real-time PCR. Inactivation of *ERK2* strongly inhibited *RANKL* expression in *ERK1*$^{-/-}$; *ERK2*$^{flox/flox}$ rib chondrocytes (E) and calvarium osteoblasts (F) in vitro. RNA was extracted from *ERK1*$^{-/-}$; *ERK2*$^{flox/flox}$ chondrocytes and osteoblasts 5 days and 8 days after infection with Ad expressing Cre recombinase or GFP. (G) ELF97-based fluorescent TRAP staining (green fluorescence) in combination with immunofluorescence for ERK protein (red fluorescence), showing the presence of ERK protein in TRAP-positive osteoclasts (arrows) in the femoral metaphysis of an *ERK1*$^{-/-}$; *ERK2*$^{flox/flox}$; *Prx1-Cre* mouse at P0. The immunofluorescent signal for ERK protein was indistinguishable from that of *ERK1*$^{-/-}$; *ERK2*$^{flox/flox}$ mice (data not shown). The lower panels show a magnification of an osteoclast indicated by arrowheads in the upper panels. Nuclei were visualized by DAPI (4′,6-diamidino-2-phenylindole). (H) X-Gal staining followed by TRAP staining showing no β-galactosidase activity in TRAP-positive osteoclast-like cells derived from spleen cells of *Prx1-Cre* mice harboring the *ROSA-LacZ* reporter allele (right panel). The staining results were indistinguishable from those observed for TRAP-positive osteoclast-like cells derived from control *ROSA-LacZ* reporter mice (left panel). (I) Spleen cells from *ERK1*$^{-/-}$; *ERK2*$^{flox/flox}$; *Prx1-Cre* mice formed TRAP-positive multinucleated osteoclast-like cells in the presence of M-CSF and RANKL (left panel). Nuclei were visualized by DAPI. These osteoclast-like cells express ERK protein (right panel), and the staining intensity was indistinguishable from that of osteoclast-like cells generated from spleen cells of *ERK1*$^{-/-}$; *ERK2*$^{flox/flox}$ mice (data not shown).

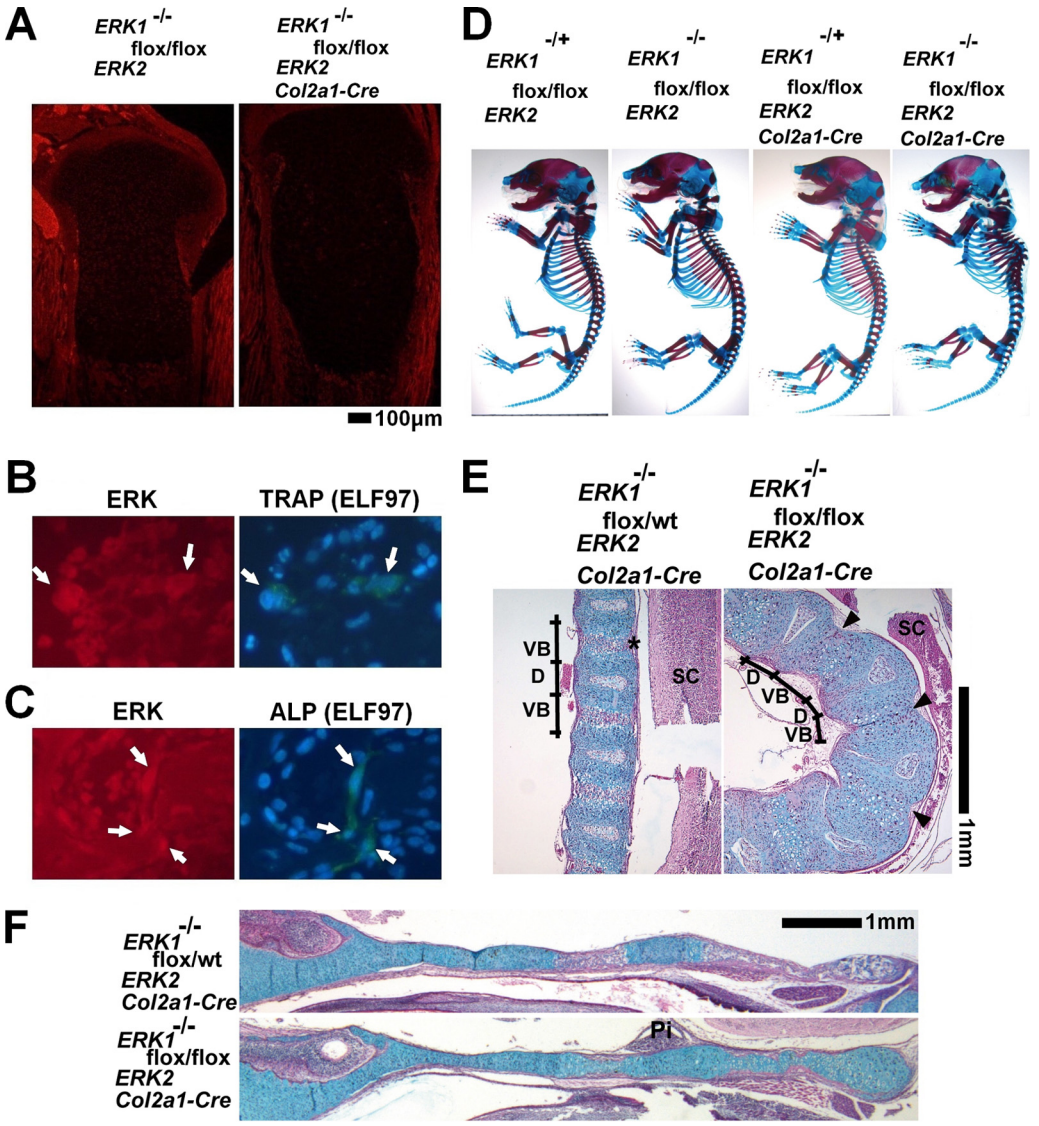

FIG. 6. *ERK1*$^{-/-}$; *ERK2*$^{flox/flox}$; *Col2a1-Cre* embryos. (A) Immunofluorescence using anti-ERK1 and ERK2 antibody showed reduced immunoreactivity in chondrocytes in the tibiae of *ERK1*$^{-/-}$; *ERK2*$^{flox/flox}$; *Col2a1-Cre* embryos at E18.5. (B) ELF97-based fluorescent TRAP staining in combination with immunofluorescence for ERK protein, showing the presence of ERK protein in TRAP-positive osteoclasts (arrows) of *ERK1*$^{-/-}$; *ERK2*$^{flox/flox}$; *Col2a1-Cre* embryos. (C) ELF97-based fluorescent alkaline phosphatase staining in combination with immunofluorescence for ERK protein, showing the presence of ERK protein in alkaline phosphatase-positive osteoblasts (arrows) of *ERK1*$^{-/-}$; *ERK2*$^{flox/flox}$; *Col2a1-Cre* embryos. (D) Skeletal preparation after alizarin red and alcian blue staining. *ERK1*$^{-/-}$; *ERK2*$^{flox/flox}$; *Col2a1-Cre* embryos showed severe kyphotic deformity in the thoracic spine at E18.5. (E, F) Hematoxylin, eosin, and alcian blue staining of the spine (E) and cranial base (F) showing an absence of ossification centers in *ERK1*$^{-/-}$; *ERK2*$^{flox/flox}$; *Col2a1-Cre* embryos at E18.5. * indicates the ossification center in the vertebral body, and arrowheads indicate the corresponding areas in *ERK1*$^{-/-}$; *ERK2*$^{flox/flox}$; *Col2a1-Cre* embryos. VB, vertebral body; D, intervertebral disc; SC, spinal cord; Pi, pituitary gland; wt, wild type.

ERK1$^{-/-}$; *ERK2*$^{flox/flox}$; *Col2a1-Cre* mice showed a strong cartilage phenotype both in the axial and in the appendicular skeletons. Skeletal preparation with alcian blue and alizarin red staining showed kyphotic deformity in the spines of *ERK1*$^{-/-}$; *ERK2*$^{flox/flox}$; *Col2a1-Cre* embryos (Fig. 6D). Histological examinations showed an absence of primary ossification centers in the spine and cranial base at E18.5 (Fig. 6E and F). In long bones, there was a gene dosage-dependent widening of the zone of hypertrophic chondrocytes (Fig. 7A). *ERK1*$^{-/-}$; *ERK2*$^{flox/flox}$; *Col2a1-Cre* embryos showed an expansion of the *Col10a1* expression domain (Fig. 7B). Similar to that in *ERK1*$^{-/-}$; *ERK2*$^{flox/flox}$; *Prx1-Cre* embryos, *Col10a1* expression was also observed in chondrocytes that were closer to the articular surface in *ERK1*$^{-/-}$; *ERK2*$^{flox/flox}$; *Col2a1-Cre* embryos, suggesting premature hypertrophy. To further confirm the role of ERK1 and ERK2 in hypertrophic differentiation of chondrocytes, we performed in vitro experiments. *ERK2* inactivation in primary *ERK1*$^{-/-}$; *ERK2*$^{flox/flox}$ chondrocytes by Ad-mediated expression of Cre recombinase resulted in increased *Col10a1* expression, further supporting the notion that ERK1 and ERK2 inhibit hypertrophic differentiation of chondrocytes (Fig. 7C). Loss of *ERK1* and *ERK2* also resulted in

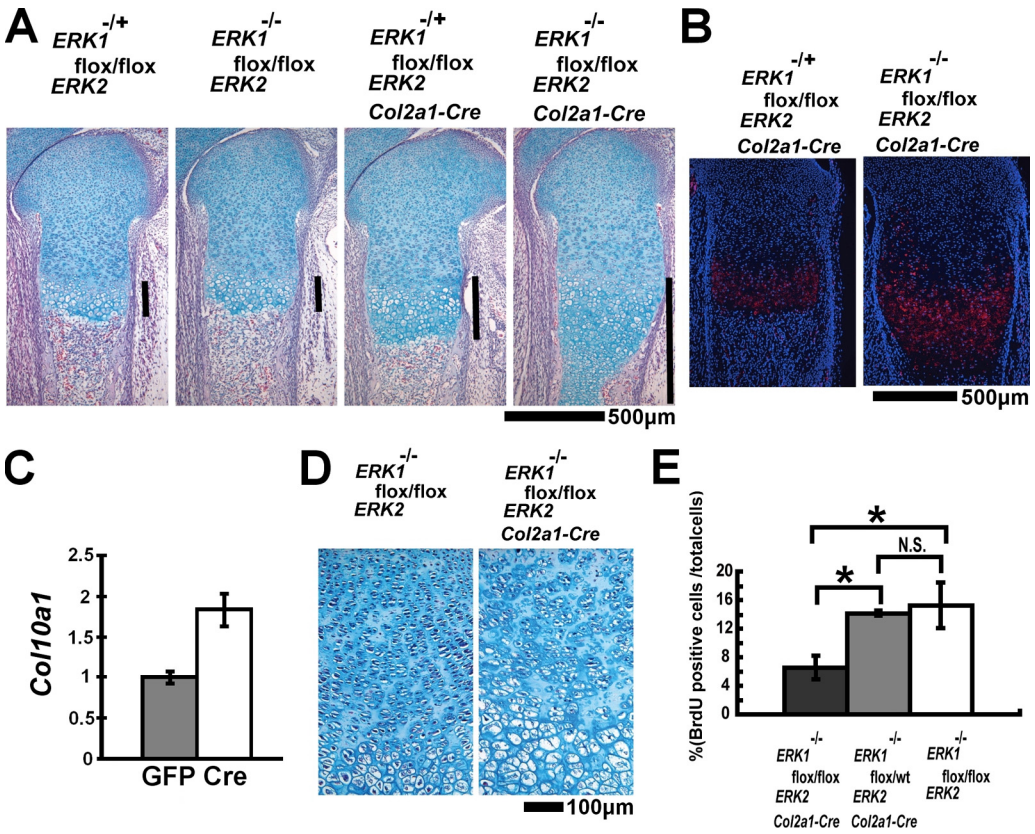

FIG. 7. (A) Hematoxylin, eosin, and alcian blue staining of the femur showing a dosage-dependent widening of the zone of hypertrophic chondrocytes at E16.5. Bars indicate the width of the zone of hypertrophic chondrocytes. (B) In situ hybridization of the tibia showing an expansion of *Col10a1*-expressing domains in *ERK1*$^{-/-}$; *ERK2*$^{flox/flox}$; *Col2a1-Cre* embryos at E18.5. (C) Primary *ERK1*$^{-/-}$; *ERK2*$^{flox/flox}$ chondrocytes were infected with Ad expressing Cre recombinase or GFP at a multiplicity of infection of 200. *Col10a1* expression was examined by real-time PCR at 5 days after Ad infection. *ERK2* inactivation in *ERK1*$^{-/-}$; *ERK2*$^{flox/flox}$ chondrocytes increased *Col10a1* expression. (D) Disorganization of columnar structures in the tibial growth plates of *ERK1*$^{-/-}$; *ERK2*$^{flox/flox}$; *Col2a1-Cre* embryos at E18.5. (E) BrdU incorporation of the distal femoral growth plate. *ERK1*$^{-/-}$; *ERK2*$^{flox/flox}$; *Col2a1-Cre* embryos showed reduced chondrocyte proliferation at E18.5. Data represent means ± standard deviations. N.S., not significant; wt, wild type. Analysis of variance was used to detect significant difference. *, $P < 0.01$.

severe disorganization of the epiphyseal cartilage. Chondrocytes failed to form columnar structures in the growth plates (Fig. 7D). BrdU incorporation experiments indicated significant reduction in chondrocyte proliferation in *ERK1*$^{-/-}$; *ERK2*$^{flox/flox}$; *Col2a1-Cre* embryos at E18.5 (Fig. 7E). These observations indicate that ERK1 and ERK2 are required for proper formation of columnar structures and chondrocyte proliferation.

Similar to those in *ERK1*$^{-/-}$; *ERK2*$^{flox/flox}$; *Prx1-Cre* embryos, TRAP-positive osteoclasts were decreased in *ERK1*$^{-/-}$; *ERK2*$^{flox/flox}$; *Col2a1-Cre* embryos at E16.5, suggesting that chondrocytes support osteoclastogenesis through ERK1 and ERK2 at this stage (Fig. 8A). The reduced osteoclastogenesis is unlikely to be due to unspecific inactivation of ERK in the osteoclast lineage, since TRAP-positive osteoclasts of *ERK1*$^{-/-}$; *ERK2*$^{flox/flox}$; *Col2a1-Cre* embryos express ERK (Fig. 6B). In addition, when osteoclast-like cells were generated in vitro from spleen cells of *Col2a1-Cre* transgenic mice harboring the *ROSA-LacZ* reporter allele, TRAP-positive osteoclast-like cells did not stain positive for X-Gal (data not shown). Furthermore, spleen cells isolated from E18.5 *ERK1*$^{-/-}$; *ERK2*$^{flox/flox}$; *Col2a1-Cre* embryos formed TRAP-positive osteoclast-like cells in the presence of M-CSF and RANKL, and these cells express ERK, similar to *ERK1*$^{-/-}$; *ERK2*$^{flox/flox}$ cells (Fig. 8B).

Increased bone formation in mice that express a constitutively active mutant of *MEK1*(*S218/222E*, Δ*32-51*) under the control of a 2.4-kb *prx1* promoter. To further examine the roles of MAPK in mesenchymal cells, we generated *Prx1-MEK1* transgenic mice that express a constitutively active mutant of *MEK1*(*S218/222E*, Δ*32-51*) and *LacZ* under the control of a 2.4-kb *prx1* promoter (Fig. 9A). X-Gal staining showed the transgene expression in the developing limb bud, the perichondrium and periosteum of the long bones, some of the periarticular chondrocytes, and the lambdoid suture in the cranium (Fig. 9B, C, and F). Protein expression of the FLAG-tagged MEK1 mutant was also confirmed by immunohistochemistry using anti-FLAG antibody (Fig. 9D). In remarkable contrast to the defective bone formation in *ERK1*$^{-/-}$; *ERK2*$^{flox/flox}$; *Prx1-Cre* mice, *Prx1-MEK1* transgenic mice showed a dramatic increase in cortical bone formation, fusion of long bones (Fig. 10A) and carpal and tarsal bones (Fig. 9E), and accelerated closure of the lambdoid suture (Fig. 9F). We observed relatively normal expression of *Gdf5* and *Wnt 14* at the presumptive joint region (data not shown), suggest-

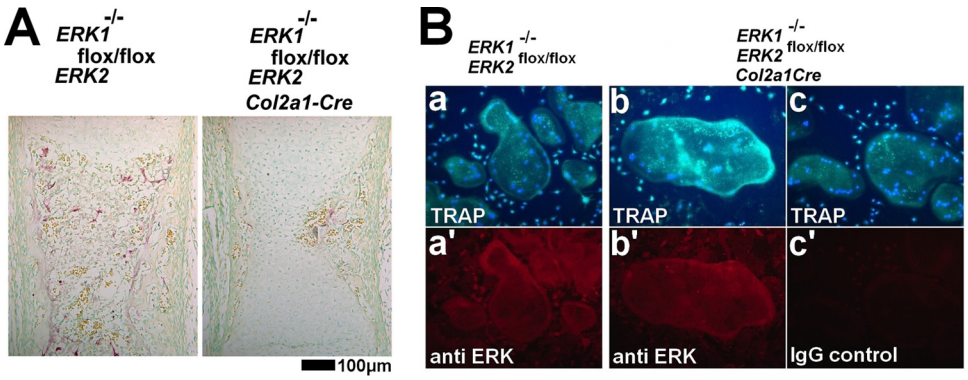

FIG. 8. (A) TRAP staining of the femur showing decreased TRAP-positive cells in *ERK1*$^{-/-}$; *ERK2*$^{flox/flox}$; *Col2a1-Cre* embryos at E16.5. (B) ELF97-based fluorescent TRAP staining in combination with immunofluorescence for ERK protein. Spleen cells from *ERK1*$^{-/-}$; *ERK2*$^{flox/flox}$ (a) and *ERK1*$^{-/-}$; *ERK2*$^{flox/flox}$; *Col2a1-Cre* (b,c) embryos formed TRAP-positive, multinucleated osteoclast-like cells in the presence of M-CSF and RANKL. Nuclei were visualized by DAPI (4′,6-diamidino-2-phenylindole). Lower panels show immunofluorescence using anti-ERK antibody (a′ and b′) or nonimmune immunoglobulin G (IgG) (c′) in corresponding cells.

ing that the bone fusions are not due to the altered joint formation but due to increased bone formation. The increase in cortical bone thickness was preceded by a thickening of the *Runx2*-, *Osterix*-, and *Bsp*-expressing perichondrium, suggesting that MAPK signaling recruits and directs osteo-chondral progenitor cells toward the osteoblastic lineage (Fig. 10B). We also observed accelerated osteocalcin expression in the perichondria of *Prx1-MEK1* transgenic mice in comparison with that in wild-type mice (see Fig. S5A in the supplemental material), suggesting an accelerated osteoblast differentiation by the increased MAPK signaling.

Inhibition of cartilage formation in Prx1-MEK1 transgenic mice. In contrast to the increased bone formation, we observed inhibition of cartilage formation in the transgenic mice. Skeletal preparation of E14.5 embryos showed a delay in the formation of cartilage anlagen, and alcian blue staining of histological sections showed smaller cartilage anlagen in the transgenic mice at E15.5 (Fig. 10C; see also Fig. S5C in the supplemental material). Immunohistochemistry for the constitutively active MEK1 indicated that cartilage develops within the transgene-expressing mesenchymal condensation (see Fig. S5B in the supplemental material). In addition, alcian blue staining was reduced in the periarticular cartilage corresponding to the expression domain of the constitutively active MEK1 (Fig. 9D). Furthermore, *Col2a1* expression was decreased in the developing cartilage primordia (Fig. 10D). Consistent with these observations in vivo, Ad-mediated expression of a constitutively active mutant of MEK1 in primary chondrocytes strongly inhibited *Col2a1* expression (Fig. 10E). In addition, FGF18, a potent activator of the MAPK pathway, also downregulated *Col2a1* expression, and the downregulation was inhibited by U0126 (Fig. 10F). Collectively, these observations indicate that increased MAPK signaling inhibits cartilage formation.

DISCUSSION

In this study, we showed that *ERK1* and *ERK2* are essential for osteoblast differentiation and bone formation. *Osteocalcin*-expressing mature osteoblasts did not develop in the absence of ERK1 and ERK2, indicating that ERK1 and ERK2 are essential for differentiation into mature osteoblasts. Despite severe impairment in osteoblast differentiation, master transcription factors for osteoblast differentiation (*Runx2*, *Osterix*, and *Atf4*) are normally expressed, indicating that ERK1 and ERK2 are not required for their expression. In addition to transcriptional regulation, ERK1 and ERK2 can regulate the activity of transcription factors posttranslationally. Indeed, Runx2 has been shown to be phosphorylated and activated by ERK MAPK (11, 43). In addition, Atf4 is phosphorylated and activated by RSK2, which is a cytoplasmic substrate of ERK1 and ERK2 (44). Phosphorylation by ERK1 and ERK2 is essential for the complete activation of RSK2 (40, 50). Therefore, reduced activity of Runx2 and Atf4 may have a role in the severe defects in osteoblast differentiation. However, downstream targets of Runx2, such as *Osterix*, *Atf4*, *Vegf*, *Ihh*, and *Col10a1*, are normally expressed in the absence of ERK1 and ERK2, suggesting that Runx2 is not totally inactive in the absence of ERK1 and ERK2 (29, 44, 48, 49, 51). In addition, the bone phenotype of *ERK1*$^{-/-}$; *ERK2*$^{flox/flox}$; *Prx1-Cre* mice is apparently more severe than that of *Atf4* and *Rsk2*-null mice, suggesting additional mechanisms for regulating osteoblast differentiation.

Consistent with this notion, we found that a number of transcription factors implicated in bone formation were downregulated in *ERK1*$^{-/-}$; *ERK2*$^{flox/flox}$; *Prx1-Cre* embryos. Notably, *Krox20*, a zinc finger transcription factor expressed in endosteal and periosteal osteoblasts, was strongly downregulated in the absence of ERK1 and ERK2. Krox20 enhances the *Osteocalcin* promoter activity (19), and *Krox20*-null mice show a strong decrease in trabecular bone formation and Osteocalcin-positive cells (20). In addition, AP-1 family members *Fra1*, *Fra2*, c-*Fos*, and *Cbfb* (which encodes a coregulator of runt-domain transcriptional factors) were all downregulated in the skeletal elements lacking ERK1 and ERK2. Since these transcriptional regulators are all implicated in bone formation (1, 9, 15, 26, 27, 47), these observations strongly suggest that ERK1 and ERK2 regulate osteoblast differentiation and bone formation through multiple regulators.

In addition to the block in osteoblast differentiation, we observed ectopic cartilage formation in the perichondria of *ERK1*$^{-/-}$; *ERK2*$^{flox/flox}$; *Prx1-Cre* mice (Fig. 4A; see also Fig.

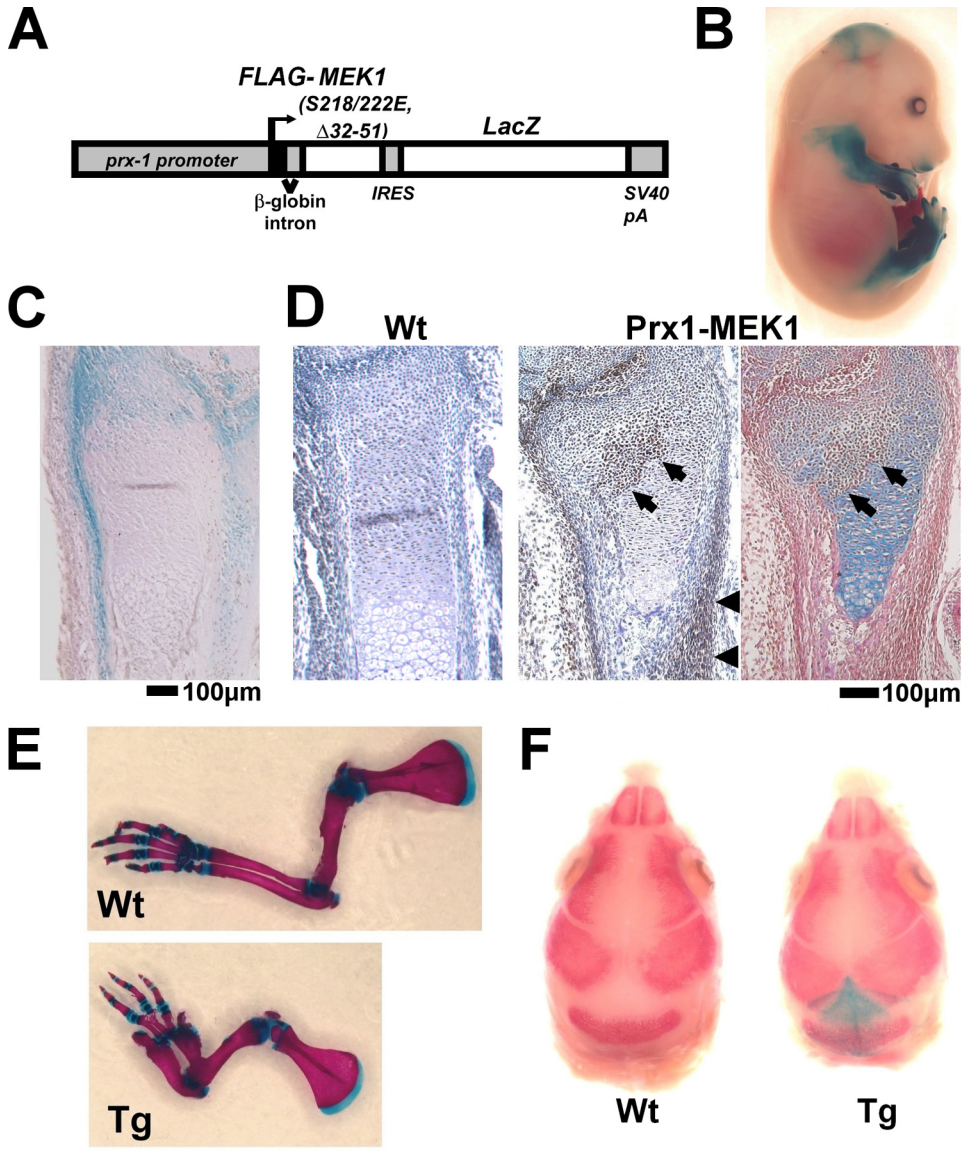

FIG. 9. (A) Schematic representation of the construct that drives the expression of a constitutively active mutant of *MEK1* and *LacZ* under the control of a 2.4-kb *prx1* promoter. (B) X-Gal staining of an E15.5 embryo showing transgene expression in the limb and cranium. (C) X-Gal staining of the distal ulna of an E15.5 embryo showing transgene expression in the periarticular chondrocytes, periosteum, and perichondrium. (D) Immunostaining of the FLAG-tagged MEK1(S218/222E, Δ32-51) using anti-M5 FLAG antibody showing transgene expression in the periarticular chondrocytes (arrows), periosteum (arrowheads), and perichondrium of the distal radius of a *Prx1-MEK1* transgenic embryo at E15.5 (middle panel). No immunoreactivity was observed in a wild-type (Wt) littermate embryo (left panel). The immunostained section was further stained with alcian blue and eosin (right panel). The cartilaginous matrix of transgene-expressing periarticular chondrocytes (arrows) shows reduced alcian blue staining. (E) Skeletal preparation of the forelimbs after alizarin red and alcian blue staining. Transgenic mice showed a thickening and shorting of long bones at P8. Wt, wild type; Tg, transgenic. (F) Skeletal preparation of the cranium after X-Gal and alizarin red staining showing transgene expression in the mesenchyme of the lambdoid suture. Transgenic mice showed an accelerated closure of the lambdoid suture at E17.5.

S2 in the supplemental material). These observations suggest that osteochondral progenitor cells were blocked in their differentiation into osteoblasts and differentiated into chondrocytes. A similar phenotype has been reported to occur in β-*catenin* conditional knockout mice (7, 12). We observed decreased β-catenin protein levels in the perichondria of *ERK1*$^{-/-}$; *ERK2*$^{flox/flox}$; *Prx1-Cre* mice. Consistent with this observation, expression of *Tcf1* and *Dkk1*, which is dependent on β-catenin signaling, was strongly inhibited in these mice. These results suggest a role for reduced β-catenin signaling in ectopic cartilage formation in the perichondrium. Loss of ERK1 and ERK2 may result in low β-catenin protein levels through intracellular cross talk between ERK and canonical Wnt signaling. Such interaction has been reported to occur in hepatocellular carcinoma, in which ERK inactivates GSK-3β, leading to the stabilization of β-catenin (8). Alternatively, the effect of ERK inactivation on β-catenin expression may be indirect, and loss of ERK1 and ERK2 results in a block in

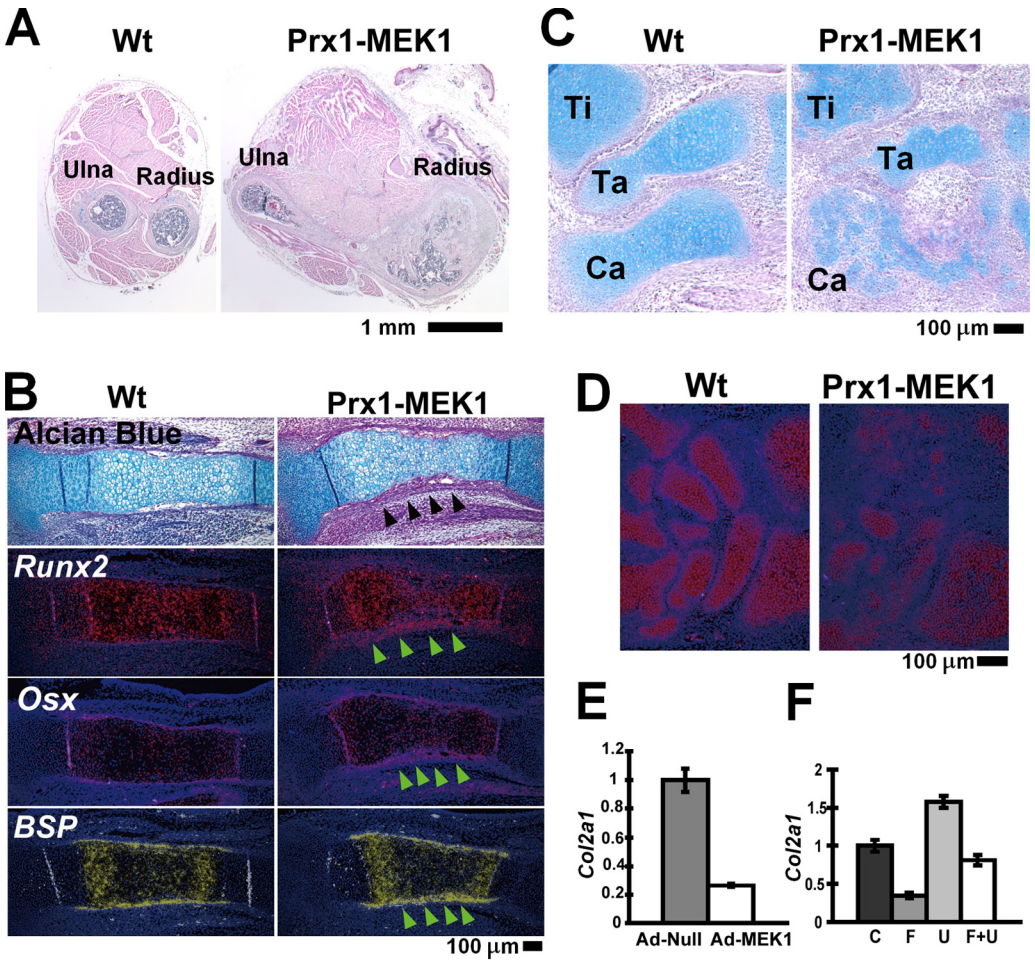

FIG. 10. (A) Cross section of the forelimb stained with hematoxylin and eosin. *Prx1-MEK1* transgenic mice showed increased bone formation and fusion of long bones (arrowhead) at P10. Wt, wild type. (B) Hematoxylin, eosin, and alcian blue staining and in situ hybridization of the tibia at E15.5. *Prx1-MEK1* transgenic embryos showed a thickening of the perichondrium, which expresses *Runx2*, *Osterix* (*Osx*), and *Bone sialoprotein* (*BSP*) (arrowheads). (C) Hematoxylin, eosin, and alcian blue staining of the foot. *Prx1-MEK1* transgenic embryos showed a delay in the formation of cartilage anlage at E15.5. Ti, tibia; Ta, talus; Ca, calcaneus. (D) In situ hybridization of the carpal bones. *Prx1-MEK1* transgenic embryos showed reduced *Col2a1* expression at E15.5. (E) Primary wild-type chondrocytes were infected with Ad expressing a constitutively active mutant of MEK1 (Ad-MEK1) or empty virus (Ad-Null). *Col2a1* expression was examined by real-time PCR at 48 h after Ad infection. Expression of a constitutively active mutant of MEK1 strongly inhibited *Col2a1* expression. (F) FGF18 treatment (20 ng/ml) downregulated *Col2a1* expression in wild-type primary chondrocytes at 24 h. The downregulation was inhibited by U0126. C, control; F, FGF18; U, U0126; F+U, FGF18 plus U0126.

osteoblast differentiation before differentiating osteoblasts express β-catenin at an increased level. The inactivation of β-catenin in calvarial mesenchymal cells by use of the *Prx1-Cre* or *Dermo1-Cre* transgene caused chondrogenic differentiation (7, 12). In contrast, loss of ERK1 and ERK2 did not cause ectopic cartilage formation in the calvaria, indicating distinct roles in the lineage specification of cranial mesenchyme. Further investigation is necessary to elucidate the interaction between MAPK and β-catenin in the lineage specification of mesenchymal cells.

In remarkable contrast to the defective bone formation in *ERK1*$^{-/-}$; *ERK2*$^{flox/flox}$; *Prx1-Cre* mice, *Prx1-MEK1* transgenic mice that express a constitutively active mutant of MEK1 in the perichondrium/periosteum showed a dramatic increase in cortical bone formation. The increase in cortical bone thickness was preceded by a thickening of the *Runx2*-, *Osterix*-, and *Bsp*-expressing perichondrium, suggesting that MAPK signaling recruits and directs osteo-chondral progenitor cells toward the osteoblastic lineage. In addition, *Prx1-MEK1* transgenic mice showed a delay in the formation of cartilage anlage. This is consistent with the notion that MAPK signaling inhibits chondrogenic differentiation of mesenchymal cells. Interestingly, the accelerated cranial suture closure and bone fusions in *Prx1-MEK1* transgenic mice were similar to those of human skeletal syndromes caused by activating mutations in fibroblast growth factor receptor 2 (14). These include Apert, Pfeiffer, Jackson-Weiss, and Crouzon syndromes. These syndromes show craniosynostosis and variable degrees of limb abnormalities, including cutaneous and osseous syndactyly and fusion of various bones. Since the MAPK pathway is one of the major downstream pathways of FGF signaling, these observations suggest that the MAPK pathway is responsible for some of the clinical features of fibroblast growth factor receptor 2-related skeletal syndromes. This notion is further supported by the

recent observation in mice that express an Apert syndrome mutation, S252W, in which MEK inhibitor U0126 treatment rescued craniosynostosis (39).

In contrast to osteoblast differentiation, loss of ERK1 and ERK2 did not affect the formation of cartilage anlage, indicating that ERK1 and ERK2 are dispensable for cartilage formation. However, loss of ERK1 and ERK2 caused severe disorganization of the epiphyseal cartilage and significant reduction in chondrocyte proliferation. These observations indicate that ERK1 and ERK2 are required for proper organization of the epiphyseal cartilage and chondrocyte proliferation. The cartilage phenotype of *ERK1*, *ERK2* conditional knockout mice was substantially alleviated by one functional allele of either ERK1 or ERK2, indicating that one allele of either ERK1 or ERK2 is sufficient for restoring the growth plate architecture and chondrocyte proliferation. We have previously shown that chondrocyte proliferation is not affected in mice that express a constitutively active mutant of MEK1 in chondrocytes (28). Apparently, basal MAPK signaling is sufficient for chondrocyte proliferation, and further increasing MAPK signaling does not stimulate proliferation. Recently, B-*raf* was conditionally inactivated in chondrocytes in the A-*raf*-null background (33). Surprisingly, these mice did not show obvious cartilage abnormalities. Our results support the notion that intact C-*raf* signaling activates ERK1 and ERK2 to a level sufficient for normal cartilage development.

In both *ERK1*$^{-/-}$; *ERK2*$^{flox/flox}$; *Prx1-Cre* mice and *ERK1*$^{-/-}$; *ERK2*$^{flox/flox}$; *Co2a1-Cre* embryos, we observed premature *Col10a1* expression in chondrocytes in the epiphysis, suggesting accelerated hypertrophic differentiation. Interestingly, *Col10a1*-positive chondrocytes were observed mainly at the lateral edges of the epiphysis in *ERK1*$^{-/-}$; *ERK2*$^{flox/flox}$; *Prx1-Cre* embryos, while chondrocytes in the center expressed *Col10a1* at lower levels. This might be related to the timing of ERK inactivation using the *Prx1-Cre* transgene. The inactivation of ERK1 and ERK2 upregulated *Col10a1* expression in chondrocytes in vitro, further supporting the notion that ERK1 and ERK2 inhibit hypertrophic differentiation. These observations are consistent with our previous observations that increased MEK1 signaling in chondrocytes inhibits hypertrophic differentiation in transgenic mice (28).

Another important function of ERK1 and ERK2 revealed in this study is the role of ERK1 and ERK2 in supporting osteoclastogenesis. Osteoclast formation is stimulated by RANKL that is secreted from osteoblasts, osteoblast precursor cells, and bone marrow stromal cells, and its action is counterbalanced by its decoy receptor OPG (3, 16, 45). Our in vitro analyses indicated that ERK1 and ERK2 are required for *RANKL* expression both in the osteoblast and in the chondrocyte lineages. Consistent with this observation, loss of ERK1 and ERK2 in the developing skeleton caused a strong decrease in *RANKL* expression and reduced formation of osteoclasts. Most interestingly, chondrocyte-specific inactivation of ERK1 and ERK2 resulted in reduced osteoclastogenesis. Similar decreases in *RANKL* expression and osteoclast formation have been shown to occur in mice in which *VDR* is conditionally inactivated in chondrocytes (25). These observations indicate that chondrocytes regulate osteoclast formation at the developing primary ossification center. Our results indicate that ERK1 and ERK2 play essential roles in supporting osteoclastogenesis through *RANKL* expression.

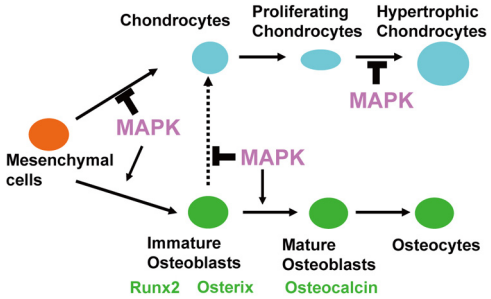

FIG. 11. Model for the roles of MAPK in chondrocyte and osteoblast differentiation. While MAPK inhibits chondrogenic differentiation of osteo-chondroprogenitor cells, MAPK enhances osteoblast differentiation. MAPK is essential for osteoblast differentiation into *Osteocalcin*-expressing mature osteoblasts. MAPK also inhibits hypertrophic chondrocyte differentiation.

In summary, our results demonstrate that ERK1 and ERK2 are essential for osteoblast differentiation, and ERK1 and ERK2 inhibit chondrogenic differentiation in the perichondrium (Fig. 11). Increased MAPK signaling promotes differentiation of mesenchymal cells into osteoblasts and inhibits chondrogenic differentiation. On the basis of these observations, we propose that ERK1 and ERK2 play essential roles in the lineage specification of mesenchymal cells. Furthermore, ERK1 and ERK2 regulate *RANKL* expression both in the osteoblast and in the chondrocyte lineages, which in turn regulates osteoclast formation. Further analyses will provide novel insights into the roles of MAPK in mesenchymal cells and skeletal development.

ACKNOWLEDGMENTS

We thank J. Martin for *Prx1-Cre* mice and the 2.4-kb *Prx1* promoter. We are grateful to M. Kurosaka for his continuous support for this work. We also thank Edward Greenfield for reagents and technical suggestions, Yoichi Ezura and Guang Zhou for critical reading of the manuscript, and Valerie Schmedlen for editorial assistance.

This work was supported by research grant no. 6-FY06-341 from the March of Dimes Birth Defects Foundation and NIH grants R21DE017406 and R01AR055556 to S.M.

REFERENCES

1. **Banerjee, C., J. L. Stein, A. J. Van Wijnen, B. Frenkel, J. B. Lian, and G. S. Stein.** 1996. Transforming growth factor-beta 1 responsiveness of the rat osteocalcin gene is mediated by an activator protein-1 binding site. Endocrinology **137:**1991–2000.
2. **Bentires-Alj, M., M. I. Kontaridis, and B. G. Neel.** 2006. Stops along the RAS pathway in human genetic disease. Nat. Med. **12:**283–285.
3. **Boyce, B. F., and L. Xing.** 2008. Functions of RANKL/RANK/OPG in bone modeling and remodeling. Arch. Biochem. Biophys. **473:**139–146.
4. **Chuderland, D., and R. Seger.** 2005. Protein-protein interactions in the regulation of the extracellular signal-regulated kinase. Mol. Biotechnol. **29:**57–74.
5. **Colnot, C.** 2005. Cellular and molecular interactions regulating skeletogenesis. J. Cell. Biochem. **95:**688–697.
6. **Cox, W. G., and V. L. Singer.** 1999. A high-resolution, fluorescence-based method for localization of endogenous alkaline phosphatase activity. J. Histochem. Cytochem. **47:**1443–1456.
7. **Day, T. F., X. Guo, L. Garrett-Beal, and Y. Yang.** 2005. Wnt/beta-catenin signaling in mesenchymal progenitors controls osteoblast and chondrocyte differentiation during vertebrate skeletogenesis. Dev. Cell **8:**739–750.
8. **Ding, Q., W. Xia, J. C. Liu, J. Y. Yang, D. F. Lee, J. Xia, G. Bartholomeusz, Y. Li, Y. Pan, Z. Li, R. C. Bargou, J. Qin, C. C. Lai, F. J. Tsai, C. H. Tsai, and M. C. Hung.** 2005. Erk associates with and primes GSK-3beta for its inactivation resulting in upregulation of beta-catenin. Mol. Cell **19:**159–170.

9. **Eferl, R., A. Hoebertz, A. F. Schilling, M. Rath, F. Karreth, L. Kenner, M. Amling, and E. F. Wagner.** 2004. The Fos-related antigen Fra-1 is an activator of bone matrix formation. EMBO J. **23:**2789–2799.
10. **Filgueira, L.** 2004. Fluorescence-based staining for tartrate-resistant acidic phosphatase (TRAP) in osteoclasts. J. Histochem. Cytochem. **52:**411–414.
11. **Ge, C., G. Xiao, D. Jiang, and R. T. Franceschi.** 2007. Critical role of the extracellular signal-regulated kinase-MAPK pathway in osteoblast differentiation and skeletal development. J. Cell Biol. **176:**709–718.
12. **Hill, T. P., D. Spater, M. M. Taketo, W. Birchmeier, and C. Hartmann.** 2005. Canonical Wnt/beta-catenin signaling prevents osteoblasts from differentiating into chondrocytes. Dev. Cell **8:**727–738.
13. **Hunziker, E. B.** 1994. Mechanism of longitudinal bone growth and its regulation by growth plate chondrocytes. Microsc. Res. Tech. **28:**505–519.
14. **Ibrahimi, O. A., E. S. Chiu, J. G. McCarthy, and M. Mohammadi.** 2005. Understanding the molecular basis of Apert syndrome. Plast. Reconstr. Surg. **115:**264–270.
15. **Jochum, W., J. P. David, C. Elliott, A. Wutz, H. Plenk, Jr., K. Matsuo, and E. F. Wagner.** 2000. Increased bone formation and osteosclerosis in mice overexpressing the transcription factor Fra-1. Nat. Med. **6:**980–984.
16. **Kim, N., P. R. Odgren, D. K. Kim, S. C. Marks, Jr., and Y. Choi.** 2000. Diverse roles of the tumor necrosis factor family member TRANCE in skeletal physiology revealed by TRANCE deficiency and partial rescue by a lymphocyte-expressed TRANCE transgene. Proc. Natl. Acad. Sci. USA **97:** 10905–10910.
17. **Kondoh, K., S. Torii, and E. Nishida.** 2005. Control of MAP kinase signaling to the nucleus. Chromosoma **114:**86–91.
18. **Kyriakis, J. M., H. App, X. F. Zhang, P. Banerjee, D. L. Brautigan, U. R. Rapp, and J. Avruch.** 1992. Raf-1 activates MAP kinase-kinase. Nature **358:**417–421.
19. **Leclerc, N., T. Noh, A. Khokhar, E. Smith, and B. Frenkel.** 2005. Glucocorticoids inhibit osteocalcin transcription in osteoblasts by suppressing Egr2/Krox20-binding enhancer. Arthritis Rheum. **52:**929–939.
20. **Levi, G., P. Topilko, S. Schneider-Maunoury, M. Lasagna, S. Mantero, R. Cancedda, and P. Charnay.** 1996. Defective bone formation in Krox-20 mutant mice. Development **122:**113–120.
21. **Logan, M., J. F. Martin, A. Nagy, C. Lobe, E. N. Olson, and C. J. Tabin.** 2002. Expression of Cre Recombinase in the developing mouse limb bud driven by a Prxl enhancer. Genesis **33:**77–80.
22. **Long, F., U. I. Chung, S. Ohba, J. McMahon, H. M. Kronenberg, and A. P. McMahon.** 2004. Ihh signaling is directly required for the osteoblast lineage in the endochondral skeleton. Development **131:**1309–1318.
23. **Marshall, C. J.** 1995. Specificity of receptor tyrosine kinase signaling: transient versus sustained extracellular signal-regulated kinase activation. Cell **80:**179–185.
24. **Martin, J. F., and E. N. Olson.** 2000. Identification of a prx1 limb enhancer. Genesis **26:**225–229.
25. **Masuyama, R., I. Stockmans, S. Torrekens, R. Van Looveren, C. Maes, P. Carmeliet, R. Bouillon, and G. Carmeliet.** 2006. Vitamin D receptor in chondrocytes promotes osteoclastogenesis and regulates FGF23 production in osteoblasts. J. Clin. Investig. **116:**3150–3159.
26. **McCabe, L. R., M. Kockx, J. Lian, J. Stein, and G. Stein.** 1995. Selective expression of fos- and jun-related genes during osteoblast proliferation and differentiation. Exp. Cell Res. **218:**255–262.
27. **Miller, J., A. Horner, T. Stacy, C. Lowrey, J. B. Lian, G. Stein, G. H. Nuckolls, and N. A. Speck.** 2002. The core-binding factor beta subunit is required for bone formation and hematopoietic maturation. Nat. Genet. **32:**645–649.
28. **Murakami, S., G. Balmes, S. McKinney, Z. Zhang, D. Givol, and B. de Crombrugghe.** 2004. Constitutive activation of MEK1 in chondrocytes causes Stat1-independent achondroplasia-like dwarfism and rescues the Fgfr3-deficient mouse phenotype. Genes Dev. **18:**290–305.
29. **Nakashima, K., X. Zhou, G. Kunkel, Z. Zhang, J. M. Deng, R. R. Behringer, and B. de Crombrugghe.** 2002. The novel zinc finger-containing transcription factor osterix is required for osteoblast differentiation and bone formation. Cell **108:**17–29.
30. **Opperman, L. A.** 2000. Cranial sutures as intramembranous bone growth sites. Dev. Dyn. **219:**472–485.
31. **Ornitz, D. M., and P. J. Marie.** 2002. FGF signaling pathways in endochondral and intramembranous bone development and human genetic disease. Genes Dev. **16:**1446–1465.
32. **Ovchinnikov, D. A., J. M. Deng, G. Ogunrinu, and R. R. Behringer.** 2000. Col2a1-directed expression of Cre recombinase in differentiating chondrocytes in transgenic mice. Genesis **26:**145–146.
33. **Provot, S., G. Nachtrab, J. Paruch, A. P. Chen, A. Silva, and H. M. Kronenberg.** 2008. A-Raf and B-Raf are dispensable for normal endochondral bone development, and parathyroid hormone-related peptide suppresses extracellular signal-regulated kinase activation in hypertrophic chondrocytes. Mol. Cell. Biol. **28:**344–357.
34. **Rodda, S. J., and A. P. McMahon.** 2006. Distinct roles for Hedgehog and canonical Wnt signaling in specification, differentiation and maintenance of osteoblast progenitors. Development **133:**3231–3244.
35. **Samuels, I. S., J. C. Karlo, A. N. Faruzzi, K. Pickering, K. Herrup, J. D. Sweatt, S. C. Saitta, and G. E. Landreth.** 2008. Deletion of ERK2 mitogen-activated protein kinase identifies its key roles in cortical neurogenesis and cognitive function. J. Neurosci. **28:**6983–6995.
36. **Seger, R., and E. G. Krebs.** 1995. The MAPK signaling cascade. FASEB J. **9:**726–735.
37. **Selcher, J. C., T. Nekrasova, R. Paylor, G. E. Landreth, and J. D. Sweatt.** 2001. Mice lacking the ERK1 isoform of MAP kinase are unimpaired in emotional learning. Learn. Mem. **8:**11–19.
38. **Shapiro, I. M., C. S. Adams, T. Freeman, and V. Srinivas.** 2005. Fate of the hypertrophic chondrocyte: microenvironmental perspectives on apoptosis and survival in the epiphyseal growth plate. Birth Defects Res. C **75:**330–339.
39. **Shukla, V., X. Coumoul, R. H. Wang, H. S. Kim, and C. X. Deng.** 2007. RNA interference and inhibition of MEK-ERK signaling prevent abnormal skeletal phenotypes in a mouse model of craniosynostosis. Nat. Genet. **39:**1145–1150.
40. **Smith, J. A., C. E. Poteet-Smith, K. Malarkey, and T. W. Sturgill.** 1999. Identification of an extracellular signal-regulated kinase (ERK) docking site in ribosomal S6 kinase, a sequence critical for activation by ERK in vivo. J. Biol. Chem. **274:**2893–2898.
41. **Soriano, P.** 1999. Generalized lacZ expression with the ROSA26 Cre reporter strain. Nat. Genet. **21:**70–71.
42. **Trivier, E., D. De Cesare, S. Jacquot, S. Pannetier, E. Zackai, I. Young, J. L. Mandel, P. Sassone-Corsi, and A. Hanauer.** 1996. Mutations in the kinase Rsk-2 associated with Coffin-Lowry syndrome. Nature **384:**567–570.
43. **Xiao, G., D. Jiang, P. Thomas, M. D. Benson, K. Guan, G. Karsenty, and R. T. Franceschi.** 2000. MAPK pathways activate and phosphorylate the osteoblast-specific transcription factor, Cbfa1. J. Biol. Chem. **275:**4453–4459.
44. **Yang, X., K. Matsuda, P. Bialek, S. Jacquot, H. C. Masuoka, T. Schinke, L. Li, S. Brancorsini, P. Sassone-Corsi, T. M. Townes, A. Hanauer, and G. Karsenty.** 2004. ATF4 is a substrate of RSK2 and an essential regulator of osteoblast biology; implication for Coffin-Lowry Syndrome. Cell **117:**387–398.
45. **Yasuda, H., N. Shima, N. Nakagawa, K. Yamaguchi, M. Kinosaki, S. Mochizuki, A. Tomoyasu, K. Yano, M. Goto, A. Murakami, E. Tsuda, T. Morinaga, K. Higashio, N. Udagawa, N. Takahashi, and T. Suda.** 1998. Osteoclast differentiation factor is a ligand for osteoprotegerin/osteoclastogenesis-inhibitory factor and is identical to TRANCE/RANKL. Proc. Natl. Acad. Sci. USA **95:**3597–3602.
46. **Yoon, S., and R. Seger.** 2006. The extracellular signal-regulated kinase: multiple substrates regulate diverse cellular functions. Growth Factors **24:** 21–44.
47. **Yoshida, C. A., T. Furuichi, T. Fujita, R. Fukuyama, N. Kanatani, S. Kobayashi, M. Satake, K. Takada, and T. Komori.** 2002. Core-binding factor beta interacts with Runx2 and is required for skeletal development. Nat. Genet. **32:**633–638.
48. **Yoshida, C. A., H. Yamamoto, T. Fujita, T. Furuichi, K. Ito, K. Inoue, K. Yamana, A. Zanma, K. Takada, Y. Ito, and T. Komori.** 2004. Runx2 and Runx3 are essential for chondrocyte maturation, and Runx2 regulates limb growth through induction of Indian hedgehog. Genes Dev. **18:**952–963.
49. **Zelzer, E., D. J. Glotzer, C. Hartmann, D. Thomas, N. Fukai, S. Soker, and B. R. Olsen.** 2001. Tissue specific regulation of VEGF expression during bone development requires Cbfa1/Runx2. Mech. Dev. **106:**97–106.
50. **Zhao, Y., C. Bjorbaek, and D. E. Moller.** 1996. Regulation and interaction of pp90(rsk) isoforms with mitogen-activated protein kinases. J. Biol. Chem. **271:**29773–29779.
51. **Zheng, Q., G. Zhou, R. Morello, Y. Chen, X. Garcia-Rojas, and B. Lee.** 2003. Type X collagen gene regulation by Runx2 contributes directly to its hypertrophic chondrocyte-specific expression in vivo. J. Cell Biol. **162:**833–842.